Nano
Engineering
Research Group

University of Illinois
at Chicago
College of Engineering

Continuum Models of Phonons in Nanostructures: Why Confined Phonon Effects are Especially Important in Selected Classes of Optoelectonic Devices --- also Some Graphene-related Results

Michael A. Stroscio[a,b,c], Richard and Loan Hill Professor
Mitra Dutta[a,b], Distinguished Professor and Interim Vice Chancellor for Research
Banani Sen[a], Ke (Robin) Xu[a], Jun Qian[a], Ke (Clare) Sun[a]

May 21, 2012, IWCE Phonon School

[a]Electrical and Computer Engineering Department, U. of Illinois at Chicago (UIC), 851 S. Morgan Street, Chicago, Illinois 60607
[b]Physics Department, U. of Illinois at Chicago, 851 S. Morgan Street, Chicago, Illinois
[c]Bioengineering Department, U. of Illinois at Chicago, 851 S. Morgan St., Chicago, IL

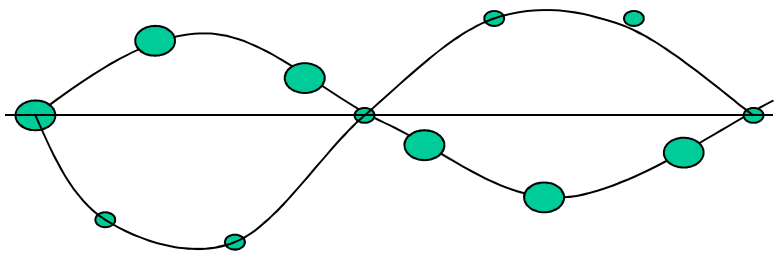

Transverse Optical (TO) Phonon

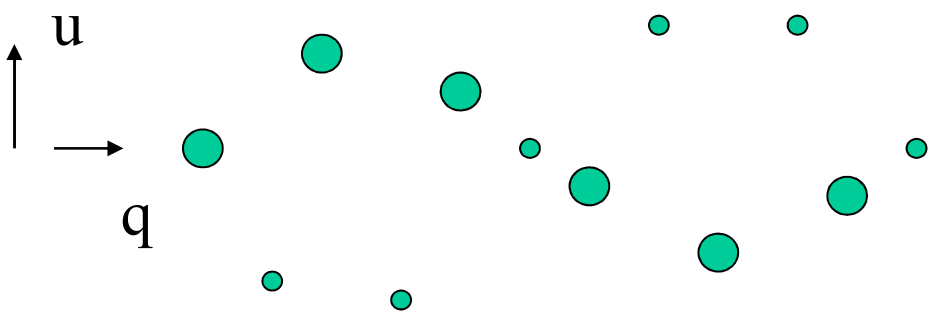

Transverse Optical (TO) Phonon
u – displacement
q - direction

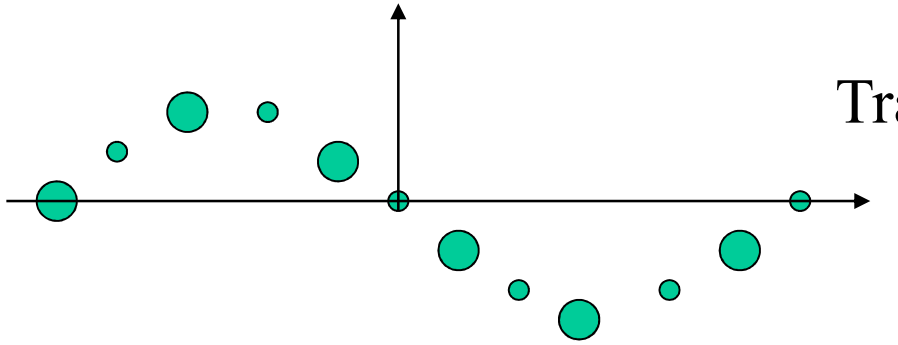

Transverse Acoustic (TA) Phonon

LO and LA Phonons have displacements along the direction of q

Phonons: Some Basic Characteristics

Boundary Conditions:

Optical modes --- continuity of the tangential component of the electric field and the z component of the displacement vector must be continuous at the interfaces

Acoustic modes --- displacement and normal component of stress tensor are continuous at interfaces

For example

$$\varepsilon_{j,z}\left.\frac{\partial\phi_j(z)}{\partial z}\right|_{z=z_j}=\varepsilon_{j+1,z}\left.\frac{\partial\phi_{j+1}(z)}{\partial z}\right|_{z=z_j}$$

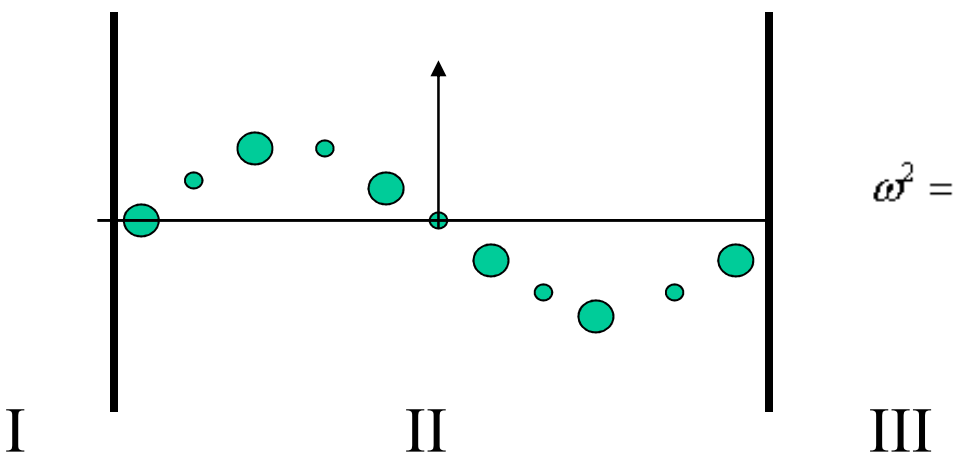

$$\omega^2=C\left(\frac{1}{M_1}+\frac{1}{M_2}\right)\pm C\sqrt{\left(\frac{1}{M_1}+\frac{1}{M_2}\right)^2-\frac{4\sin^2\left(\frac{ka}{2}\right)}{M_1M_2}}$$

↓

Quantized Confined Phonons

Normalization:

Mode amplitude normalized so that the energy in each model is the quantized phonon energy – example 2D graphene

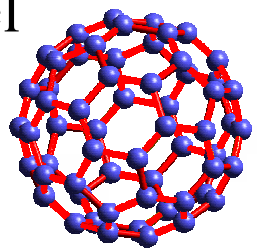

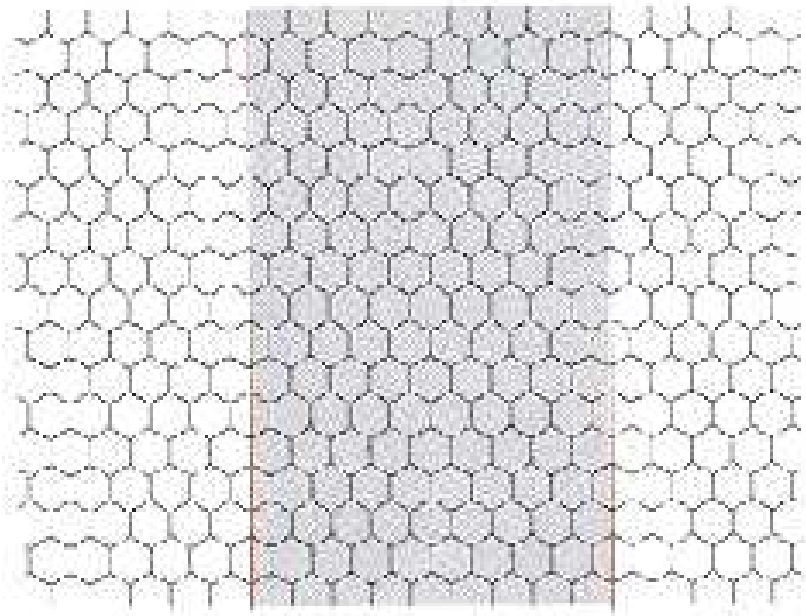

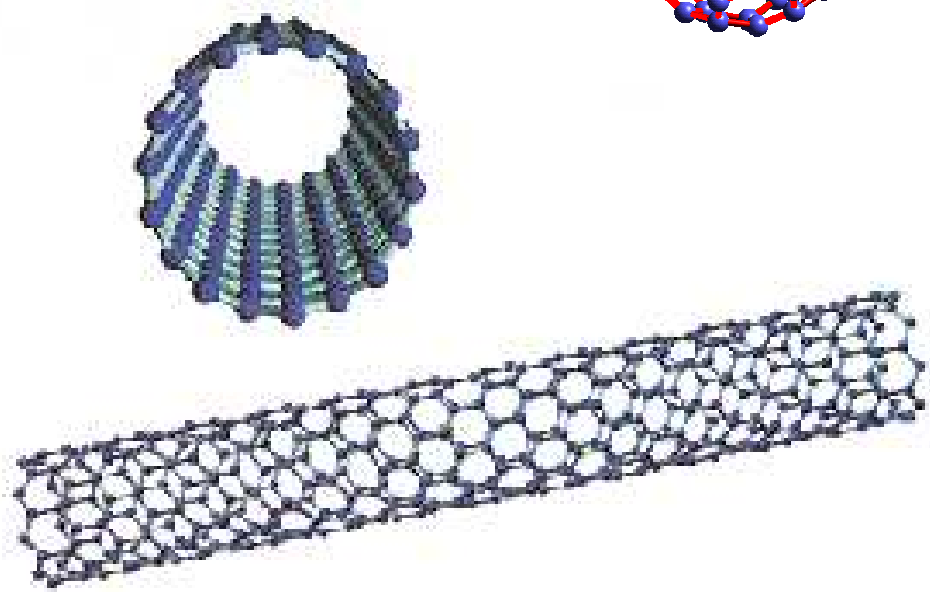

$$\frac{1}{S}\int_s \left(u\cdot u^* + v\cdot v^*\right) dxdy = \frac{\hbar}{2M\omega_{mn}^{LO}}$$

Elastic Continuum Theory Gives Correct Energy for a Dominant Mode of the Nanomechanical Modes in Carbon Nanotubes and in C_{60}

McEwen & Park et al., Nature September 2000

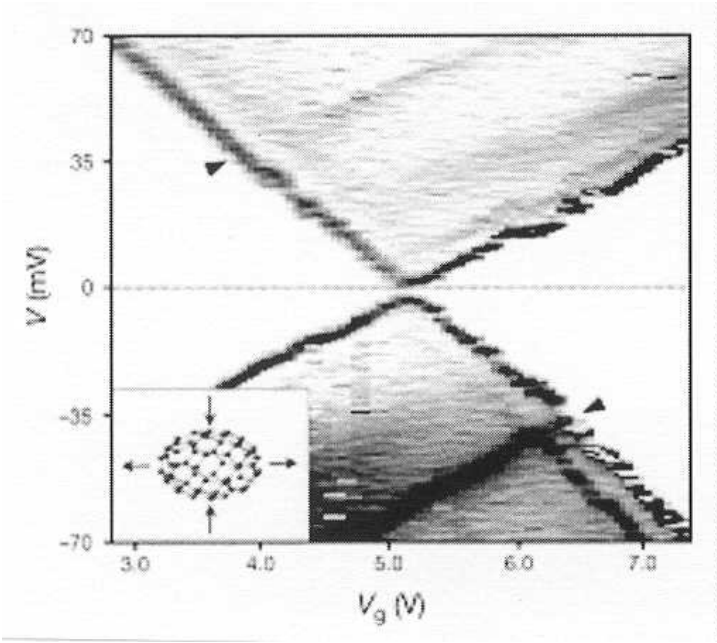

35 meV mode observed experimentally

Elastic Continuum Results

Mode	**Energy (meV)**
a_0	62
a_1	74
a_2	111
b_2	32
b_3	38

Matches our theoretical results to 10%

Goal: Theoretical Description of Nanoscale Mechanical Structures for Nanodevice and Sensor Applications including Nanocantilevers

Phonons: Some Basic Characteristics

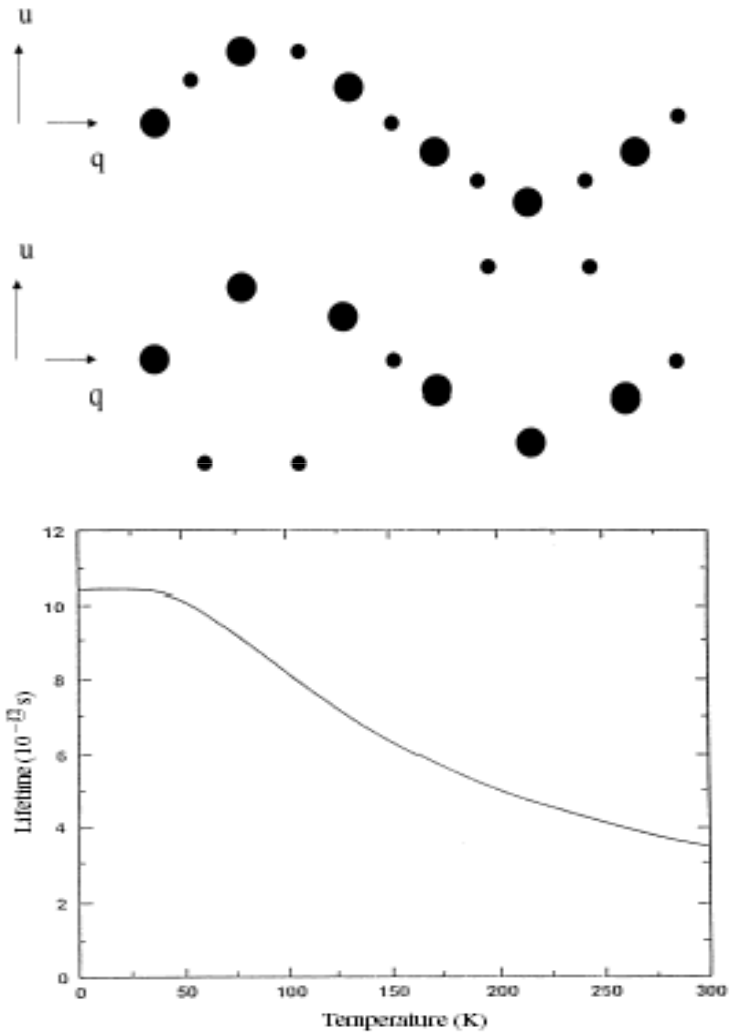

Figure 6.2. LO phonon lifetime in GaAs as a function of temperature. From Bhatt *et al.* (1994), American Institute of Physics, with permission.

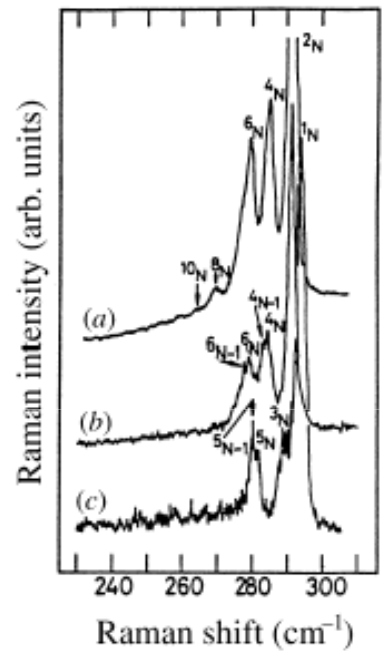

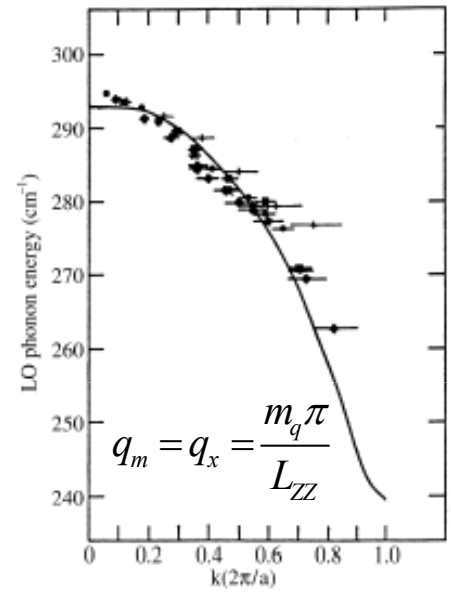

Precision and Nature of Optical Phonon Confinement
H. Sakaki et al.

Anharmonic Effects:
Klemen's Channel with Keating Model ---Bhatt, Kim and Stroscio

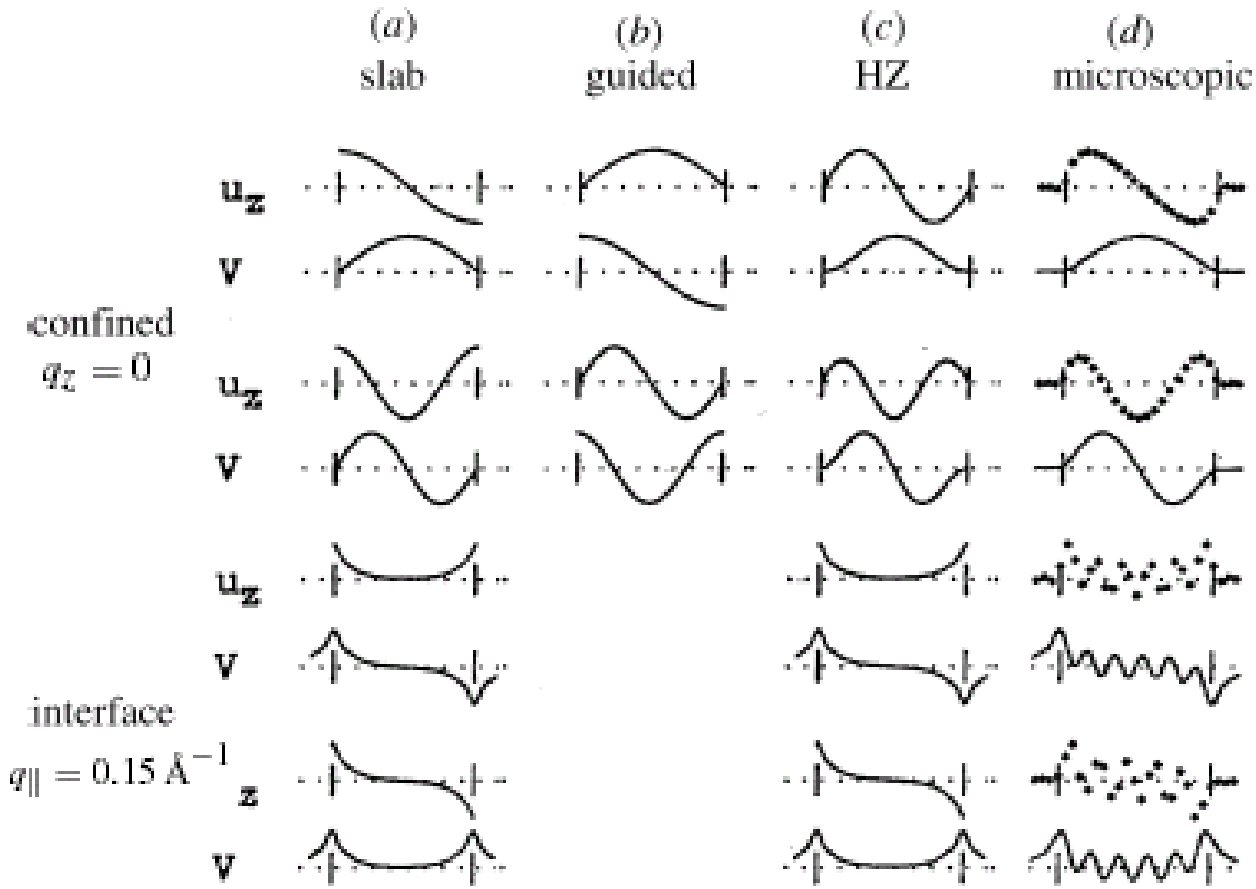

Figure C.3. The z-component of the atomic displacement, u_z, and the corresponding potential V for each of the modes reported by Rücker *et al.* (1991, 1992). The optical modes are presented for a 56 Å (001)-oriented GaAs quantum well surrounded by two AlAs layers.

Molinari et al.

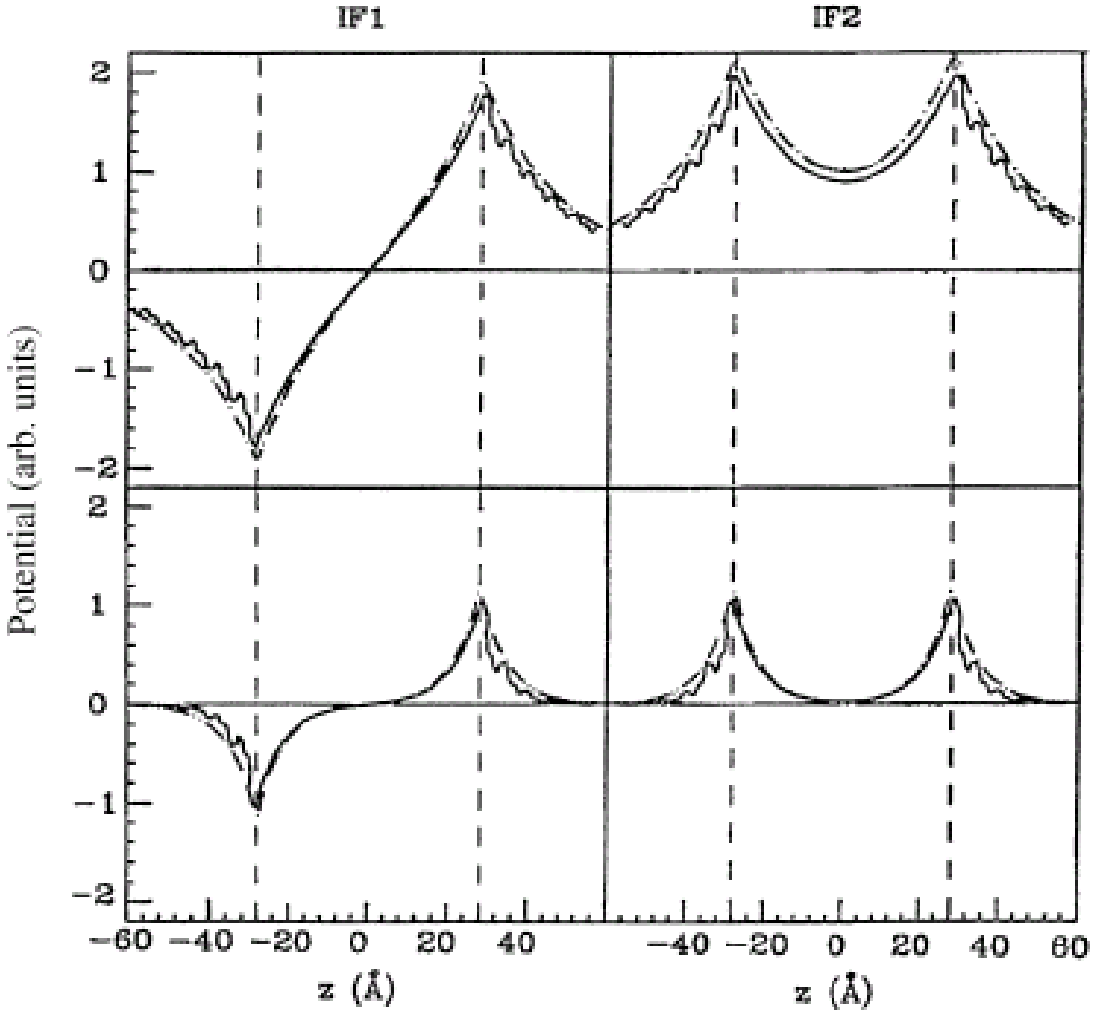

Figure C.4. Detailed comparison of potentials for the high-frequency symmetric (IF1) and antisymmetric (IF2) interface modes, as calculated via both macroscopic and microscopic models for $q = (q_X, 0, 0)$, where $q_X = 0.05$ Å^{-1} for the modes displayed in the upper half of the figure and $q_X = 0.15$ Å^{-1} for the modes displayed in the lower half of the figure.

Molinari et al.

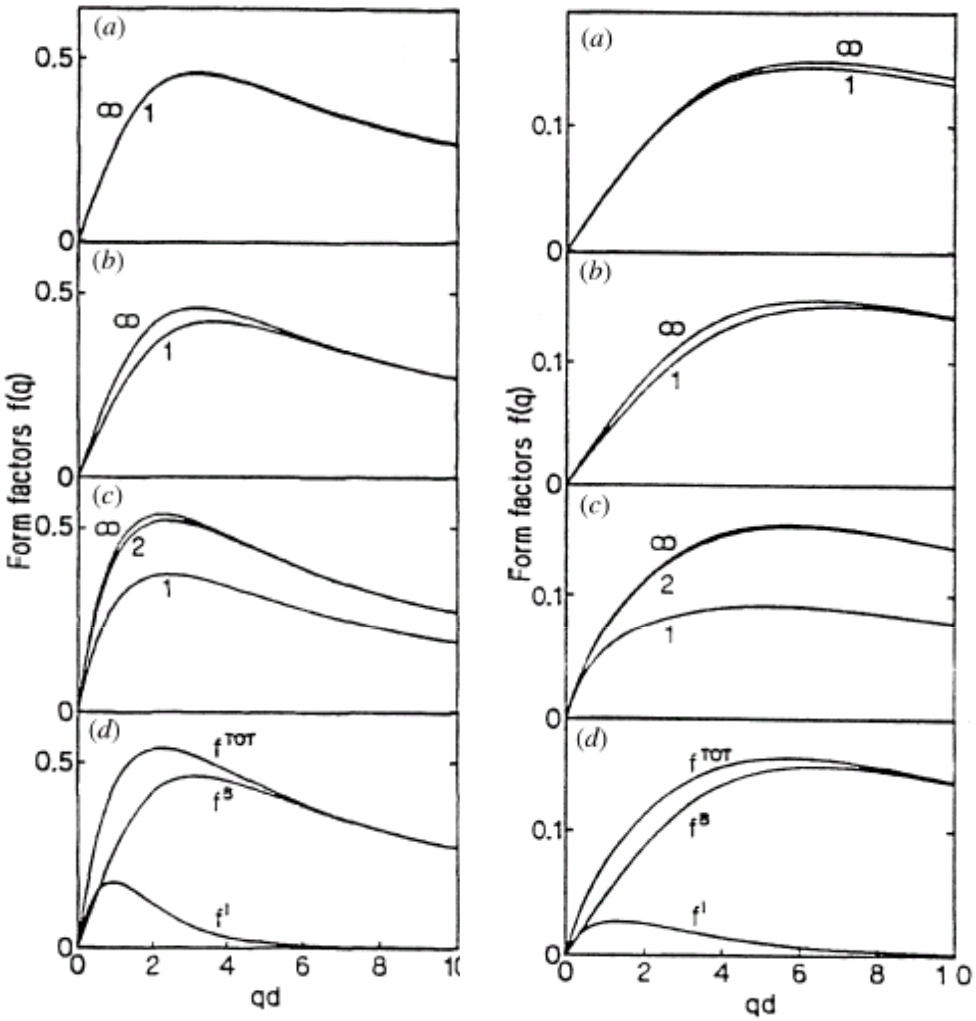

Figure C.1 for the case of intrasubband transitions and Figure C.2 for the case of intersubband transitions.

Form factors $f_n(q)$ for intrasubband scattering for optical modes in a quantum well as functions of qd for three different cases: (a) slab modes, (b) reformulated slab modes, and (c) guided modes. The labels 1,2, and ∞ designate the lowest-order mode, the second-order mode, and the infinite sum over all modes. (d) depicts the total form factor for bulk modes, f^B, as well as that for the interface modes, f^I; $f^{\text{tot}} = f^B + f^I$. From Nash (1992), American Physical Society, with permission.

Nash (1992) showed that the form factors $f_n(q)$ corresponding to the three sets of complete and orthogonal modes – slab modes plus IF modes, H–Z modes plus IF modes, and guided modes – are identical. This result is evident from Figure C.1 for the case of intrasubband transitions and Figure C.2 for the case of intersubband transitions.

Selection of Major Theoretical Papers: Optical Modes

- **R. Fuchs and K. L. Kliewer**, **"Optical Modes of Vibration in an Ionic Slab,"** Physical Review, 140, A2076-A2088 (1965).
- **J. J. Licari and R. Evrard**, **"Electron-Phonon Interaction in a Dielectric Slab: Effect of Electronic Polarizability,"** Physical Review, B15, 2254-2264 (1977).
- **L. Wendler**, **"Electron-Phonon Interaction in Dielectric Bilayer System: Effects of Electronic Polarizability,"** Physics Status Solidi B, 129, 513-530 (1985).
- **C. Trallero-Giner, F. Garcia-Moliner, V. R. Velasco, and M. Cardona**, **"Analysis of the Phenomenological Models for Long-Wavelength Polar Optical Modes in Semiconductor Layered Systems,"** Physical Review, B45, 11,944-11,948 (1992).
- **K. J. Nash**, **"Electron-Phonon Interactions and Lattice Dynamics of Optic Phonons in Semiconductor Heterostructures,"** Physical Review, B46, 7723-7744 (1992). --- For slab modes, reformulated slab vibrations, and guided modes, "intrasubband and intersubband electron-phonon scattering rates are **independent of the basis set used to describe the modes, as long as this set is orthogonal and complete**."
- **F. Comas, C. Trallero-Giner, and M. Cardona**, **"Continuum Treatment of Phonon Polaritons in Semiconductor Heterostructures,"** Physical Review, B56, 4115-4127 (1997). --- Seven coupled partial differential equations; solutions for isotropic materials; **the non-dispersive case "leads to the the Fuchs-Kliewer slab modes."**

More on Confined, Interface, and Half-Space Phonon Modes

in

Phonons and Nanostructures

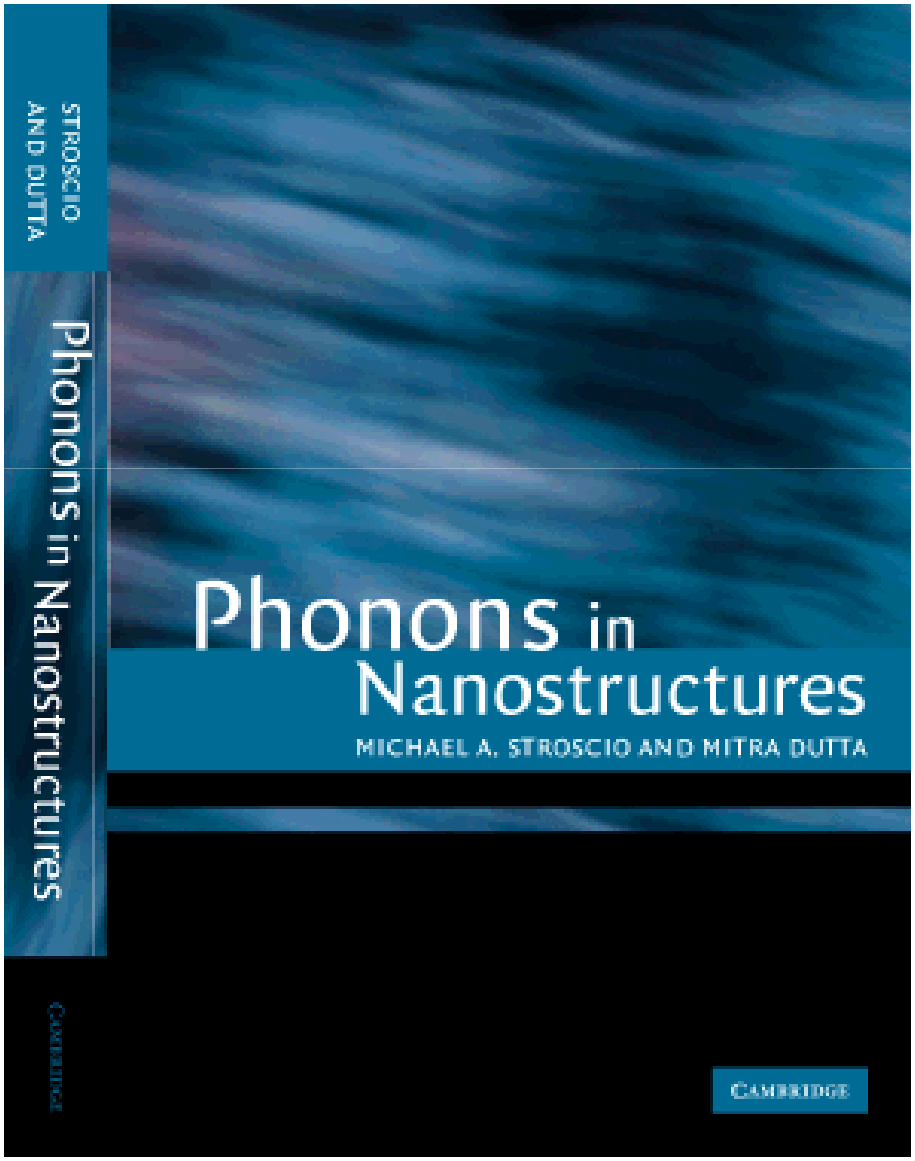

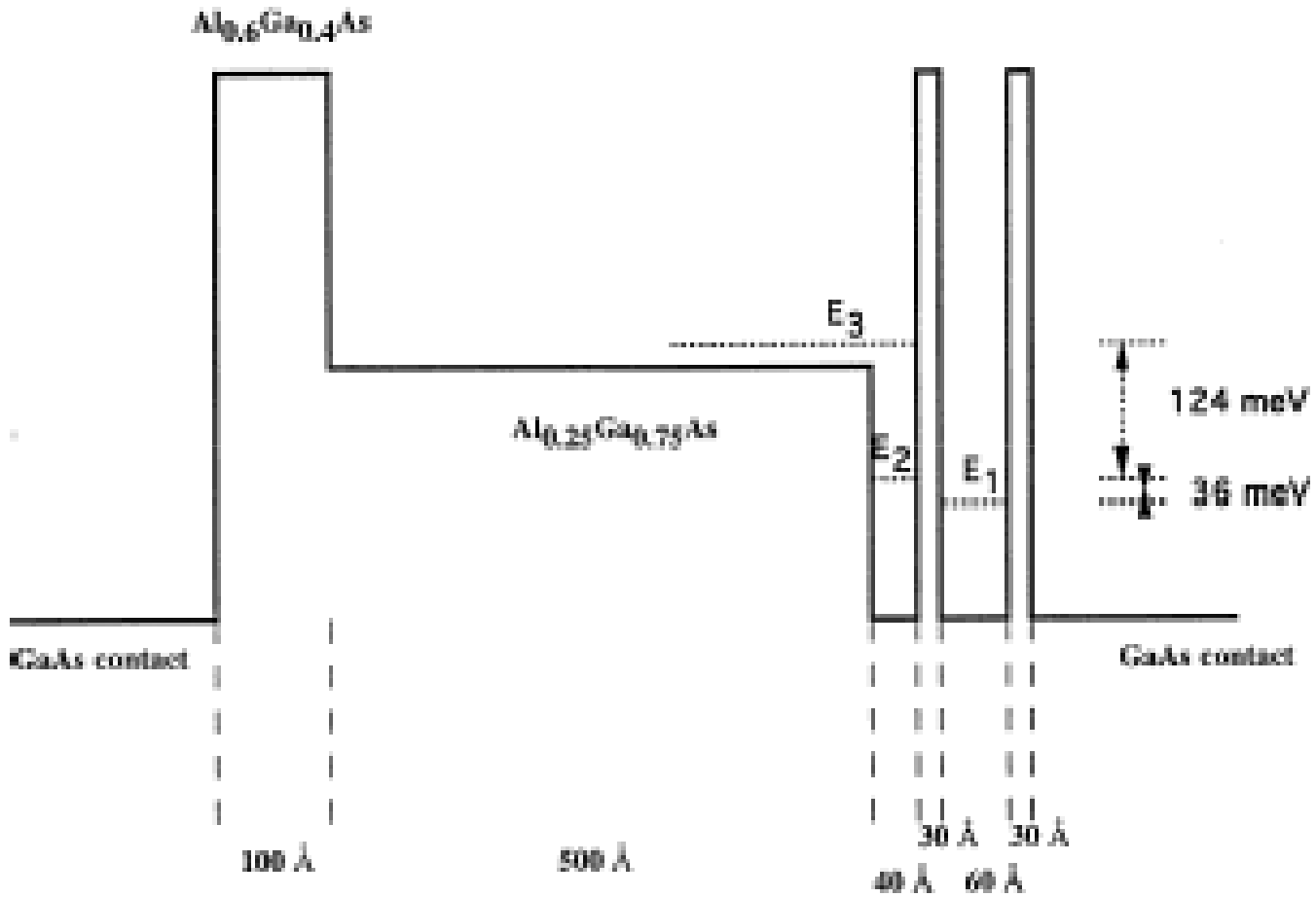
$Al_{0.6}Ga_{0.4}As$
E_3
124 meV
$Al_{0.25}Ga_{0.75}As$
E_2
E_1
36 meV
GaAs contact
GaAs contact
100 Å
500 Å
30 Å
30 Å
40 Å
60 Å

More on Interface Modes

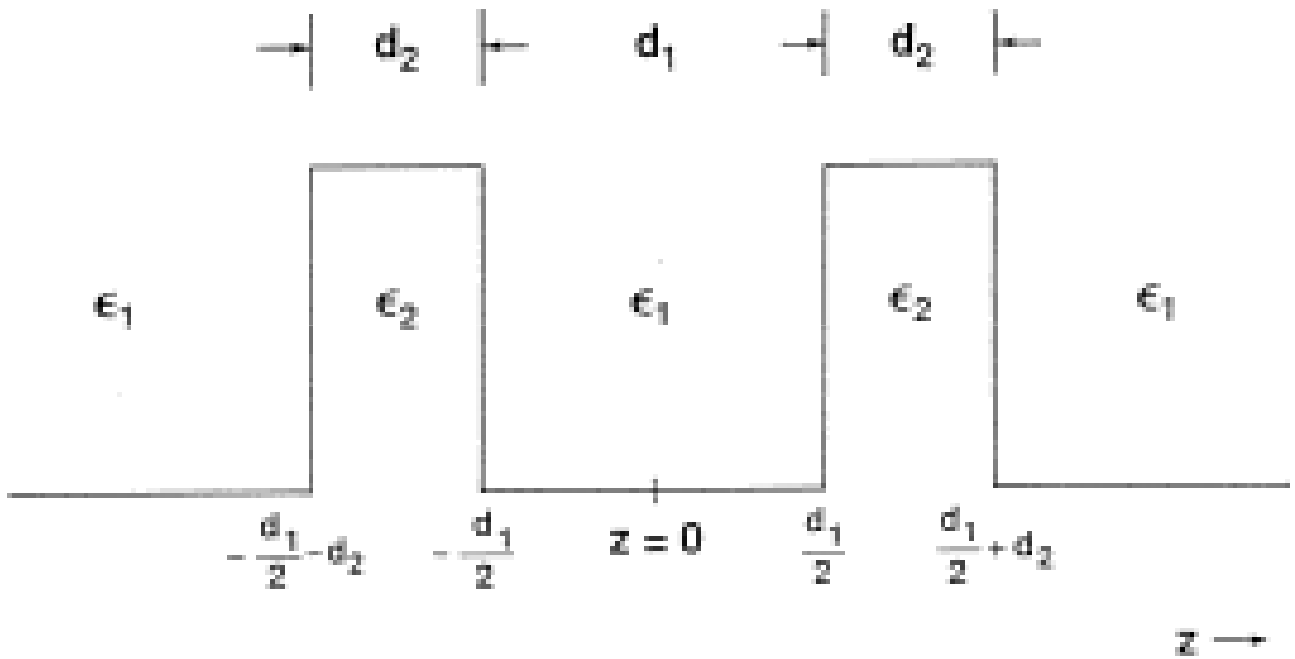

More on Interface Modes

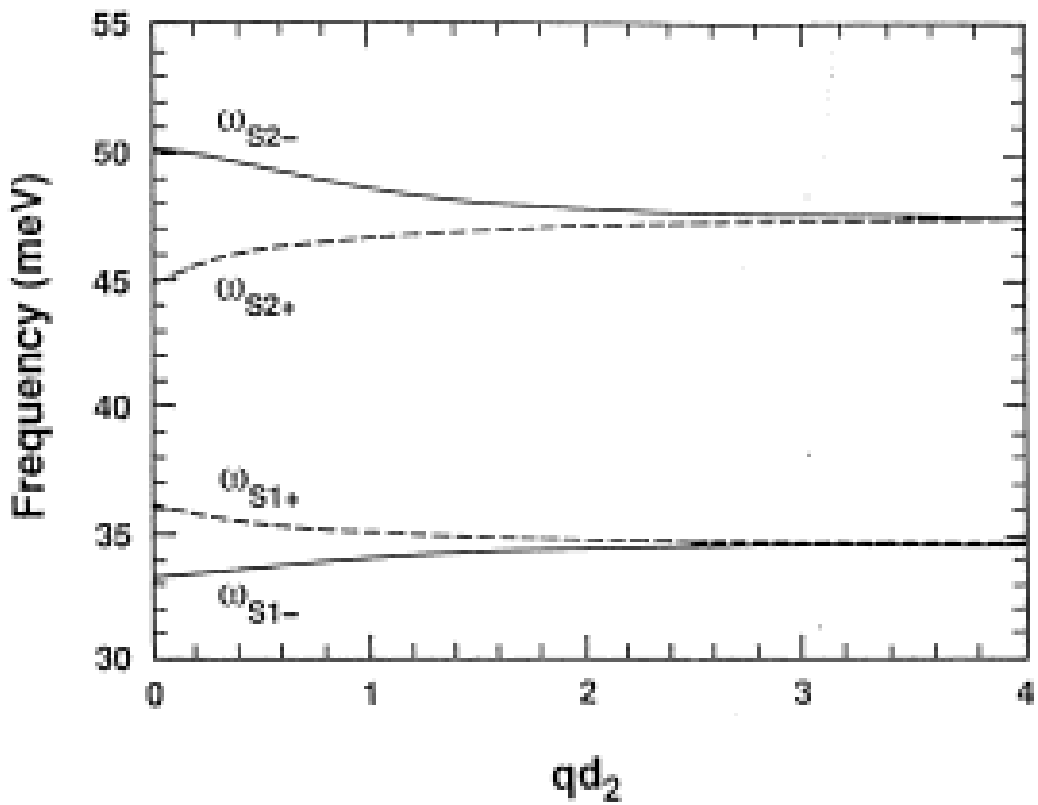

More on Interface Modes

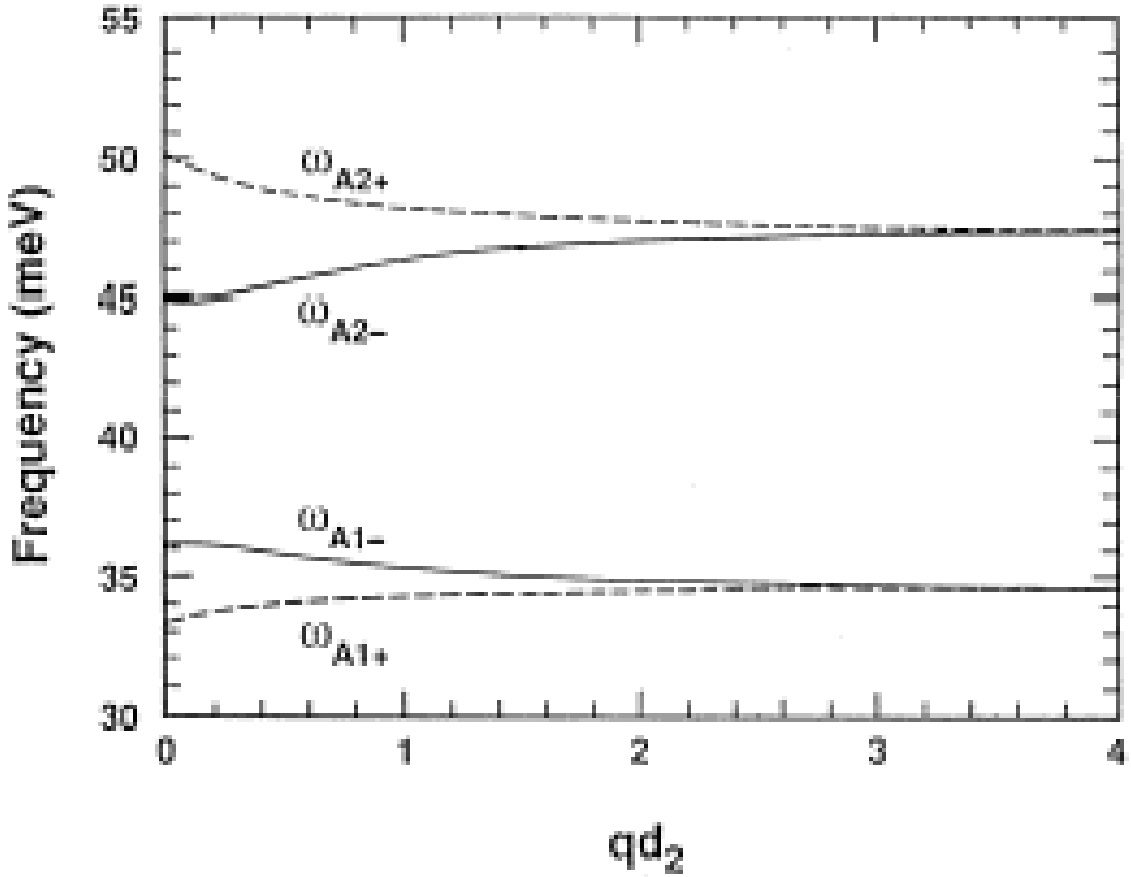

More on Interface Modes

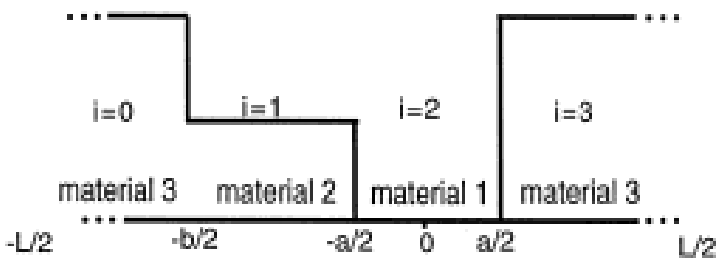

(a)

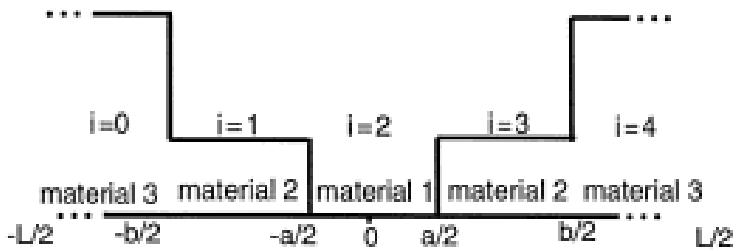

(b)

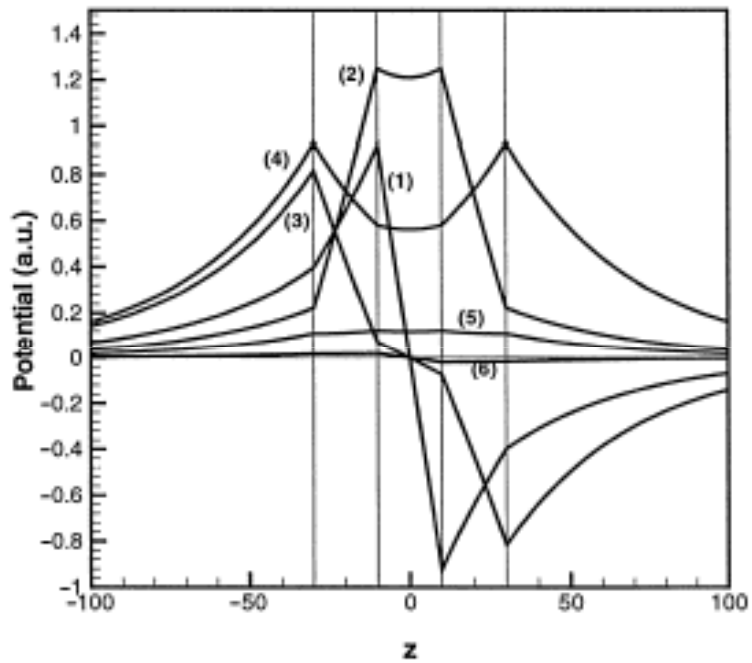

Phonon "Bands"

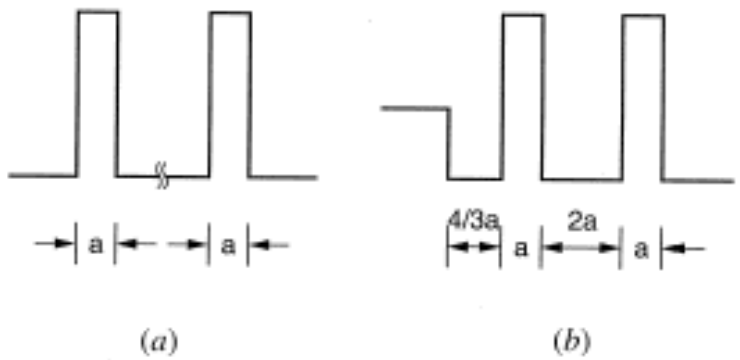

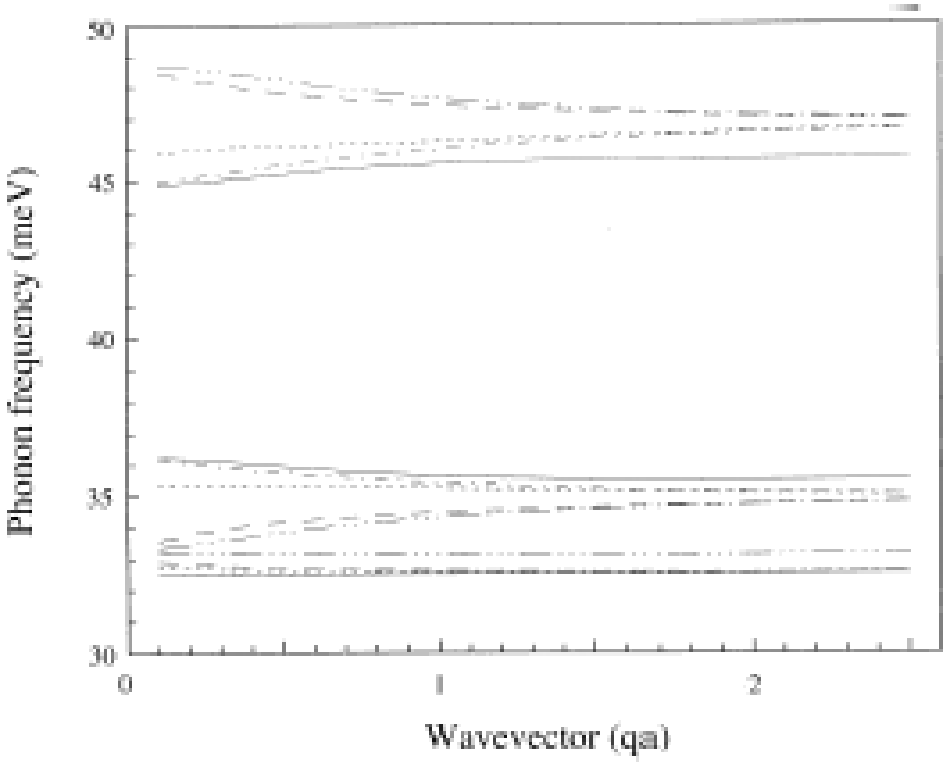

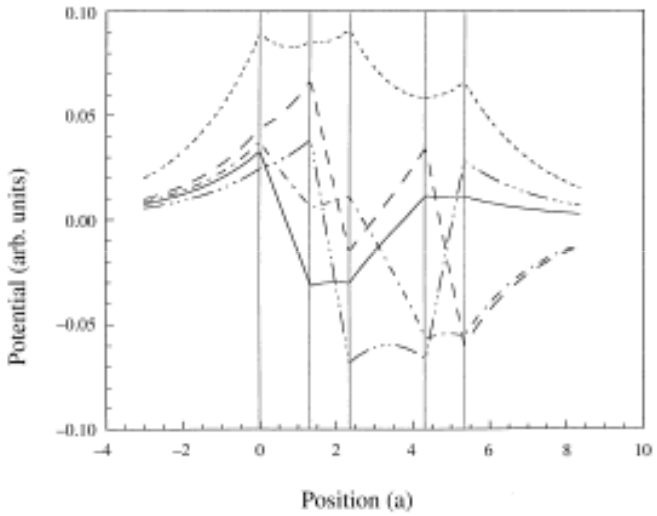

Phonon "Bands"

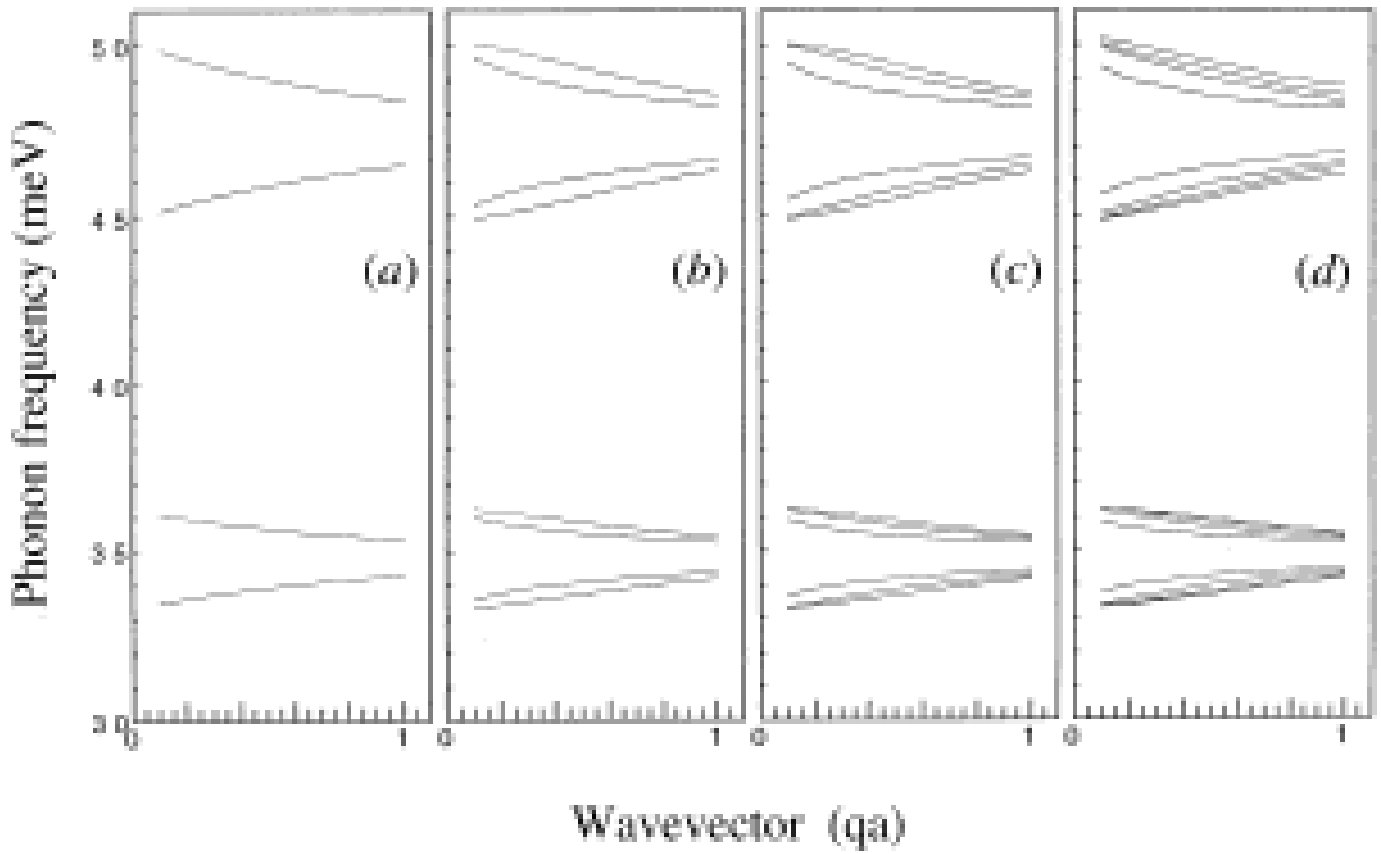

Improved Semiconductor Lasers via Phonon-Assisted Transitions

Key Point -- Optical Devices not Electronic Devices!

Why? ENERGY SELECTIVITY

A single engineered phonon mode may be selected to modify a selected interaction

Interface Optical Phonons: Applications to Phonon-Assisted Transitions in Heterojunction Lasers

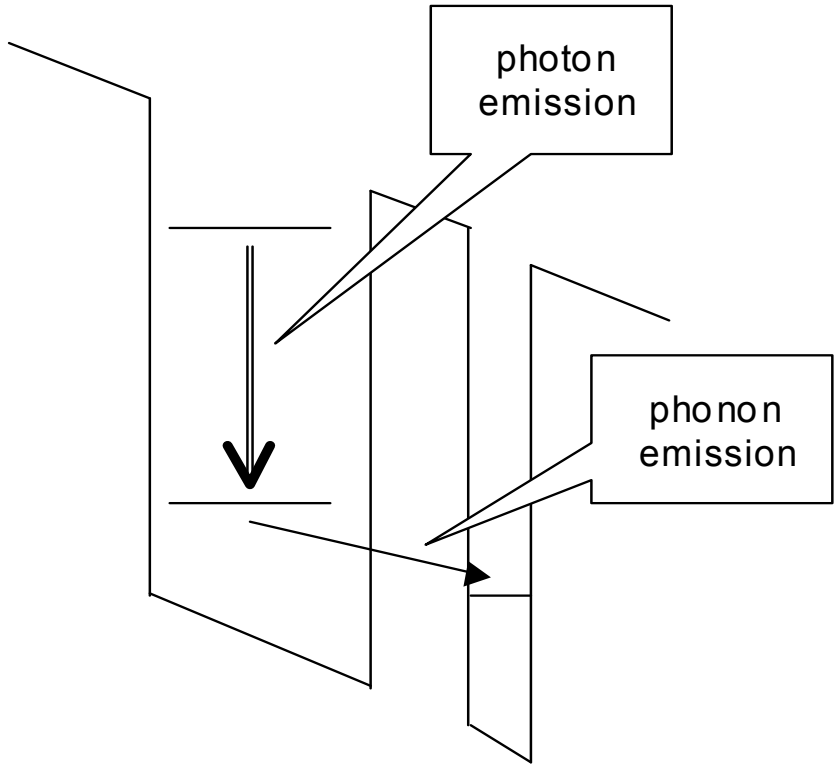

Interface-Phonon-Assisted Processes: Double Resonance Process

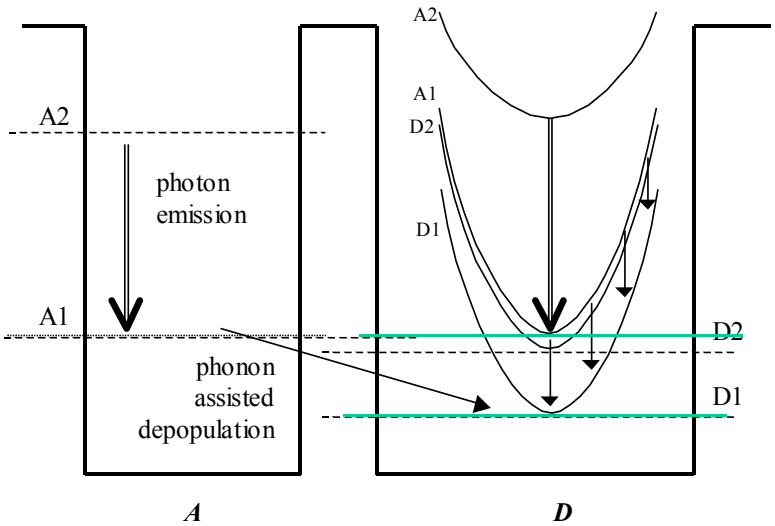

Gain enhancements greater than two orders of magnitude

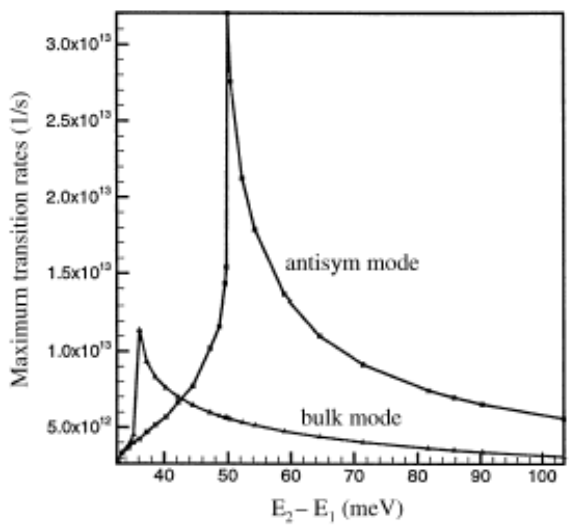

Interface phonon modes dominate over bulk modes

Nano Engineering Research Group

APPLIED PHYSICS LETTERS VOLUME 75, NUMBER 21 22 NOVEMBER 1999

Phonon enhanced inverse population in asymmetric double quantum wells

Michael A. Stroscio
U.S. Army Research Office, P.O. Box 12211, Research Triangle Park, North Carolina 27709-2211
Mikhail Kisin,[a] Gregory Belenky, and Serge Luryi
Department of Electrical and Computer Engineering, State University of New York at Stony Brook, New York 11794-2350

University of Illinois at Chicago College of Engineering

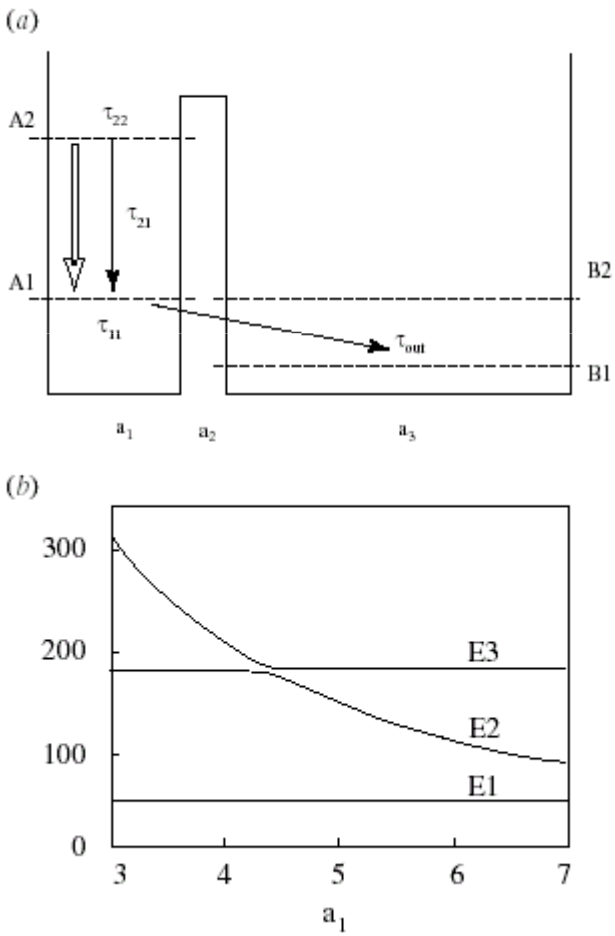

a_2 = 2 nm, a_3 = 10 nm

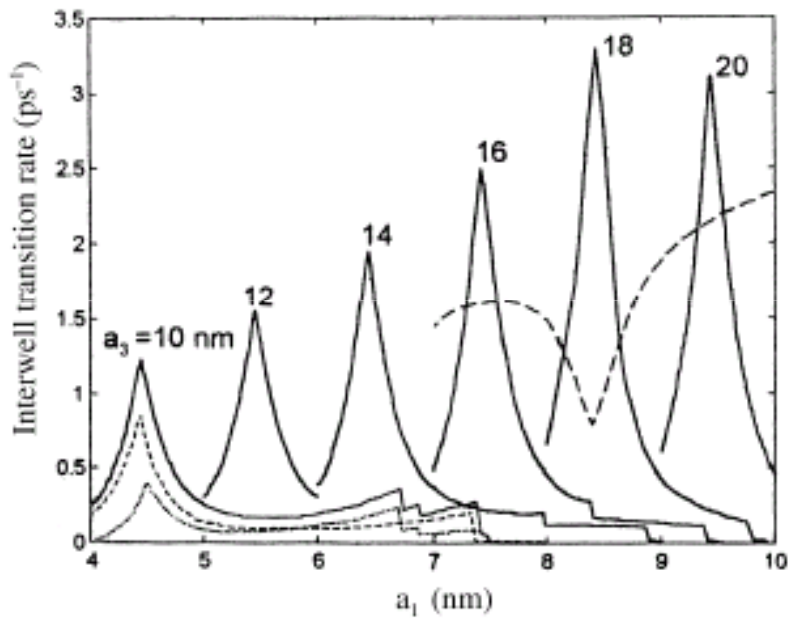

$\eta_{tot} = n_{A2} / n_{A1} = \tau_{21}/\tau_{out}$
$= 6$ for $a_1 = 8.5$ nm

$\eta_{loc} = (n_{A2} / n_{A1})_{k=0}$
$= \eta_{tot} (1 + \tau_{11}/ \tau_{out})$ EA2-A1/Ephonon
$\geq 50 - 100$

Phonon enhanced inverse population in asymmetric double quantum wells

Michael A. Stroscio
U.S. Army Research Office, P.O. Box 12211, Research Triangle Park, North Carolina 27709-2211

Mikhail Kisin,[a] Gregory Belenky, and Serge Luryi
Department of Electrical and Computer Engineering, State University of New York at Stony Brook, New York 11794-2350

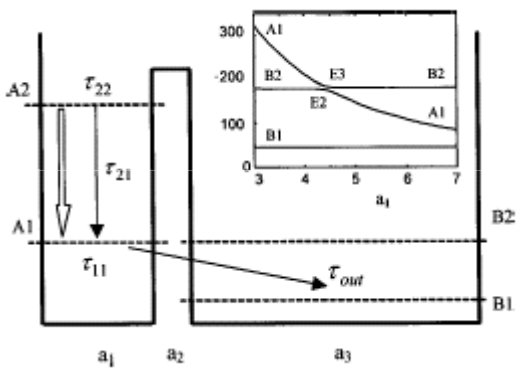

FIG. 1. Model band diagram and energy levels of an AlAs/GaAs double quantum well heterostructure. Double-lined arrow corresponds to the light-emitting transition in the heterostructure. The inset shows the positions of three lowest subbands (in meV) as a function of the narrow well width a_1 (in nm) for fixed values $a_2=2$ nm and $a_3=10$ nm.

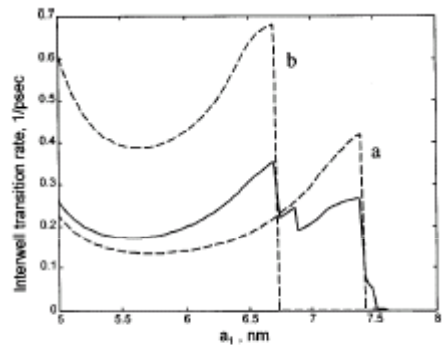

FIG. 2. Onset for the interwell electron-phonon resonance. Solid line shows the total $A1-B1$ transition rate by all confined and interface LO-phonon modes of a double quantum well heterostructure as a function of the narrow well width a_1. Here $a_2=2$ nm and $a_3=10$ nm. Two dashed curves represent the interwell transition rates calculated in the single-mode bulk-like LO-phonon spectrum approximation with phonon energies: (a) $\hbar\omega_{LO}^{GaAs}=36$ meV, and (b) $\hbar\omega_{LO}^{AlAs}=51$ meV.

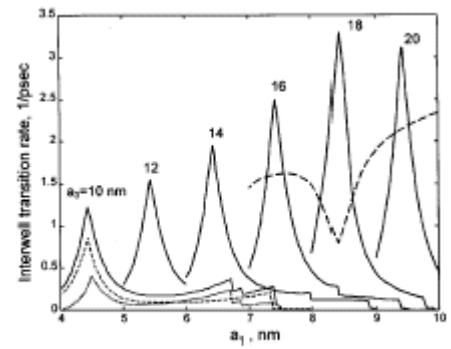

FIG. 3. Peak values of the interwell optical-phonon-assisted transition rate under the double electron-phonon resonance condition. The curves are labeled with the value of the wider quantum well width a_3 in nm. Curve 10 details individual contributions to the overall phonon-emission rate: dashed line-confined phonon modes, dotted line-interface phonon modes. Bold dashed line represents the rate of the nonradiative intrawell intersubband transitions, τ_{21}^{-1}, for the heterostructure with $a_3=18$ nm.

transitions indirect in real space.[11] The exemplary intrawell $A2-A1$ phonon-emission rate for the heterostructure with $a_3=18$ nm is shown in Fig. 3 by the bold dashed line. The total intersubband population ratio, η_{tot}, can be roughly estimated as $\eta_{tot}=n_{A2}/n_{A1}\approx\tau_{21}/\tau_{out}$ and under the double resonance condition ($a_1=8.5$ nm) it is as high as $\eta_{tot}\approx 6$, whereas outside the resonance region the total population inversion disappears. Thus for $a_1=8.0$ nm, we have only $\eta_{tot}\approx 0.5$. It is worth noting that the total subband populations determine the optical gain and the output power only in the high electron concentration limit.[12] For low electron concentrations $n_A\approx 10^{11}\,\mathrm{cm}^{-2}$, the lasing action is governed by the local nonequilibrium k-space population inversion between $A2$ and $A1$ subband bottoms which cannot be reduced to η_{tot}. In this case, the interwell depopulation rate becomes even more important. Assuming that $A2$ electrons are distributed in a narrow region near the subband bottom we have[3,12]

$$\eta_{loc}=\left(\frac{n_{A2}}{n_{A1}}\right)_{k=0}\approx\eta_{tot}\left(1+\frac{\tau_{11}}{\tau_{out}}\right)^{E_{A2A1}/\hbar\omega_{ph}}.$$

For a large $A2-A1$ separation and low values of τ_{out} the local population inversion can be significantly enhanced. For the double-quantum-well heterostructure with $a_1=8.5$ nm, $a_2=2$ nm, and $a_3=18$ nm, we find $\tau_{11}/\tau_{out}\approx 0.6$ and $E_{A2A1}/\hbar\omega_{LO}^{GaAs}\approx 5$, which results in $\eta_{loc}\approx 10\eta_{tot}$ and may be very favorable for the overall laser performance.

It should be clearly understood, however, that population inversion is not the only important parameter for a successful laser design. For instance, care must be taken to minimize the leakage of electrons from the upper lasing level $A2$ through a third energy level $B3$ of the wide well, which shunts the useful injection current. This process has little effect on the population inversion but it increases the lasing threshold. For our exemplary heterostructure, calculations show that the level $B3$ can be located within less than one $\hbar\omega_{ph}$ from the level $A2$, thus suppressing phonon-assisted leakage, by taking the active quantum well width $a_1\approx 11.5$ nm and applying an external electric field 8 kV/cm to satisfy the double electron-phonon resonance condition.

Interface-Phonon-Assisted Processes

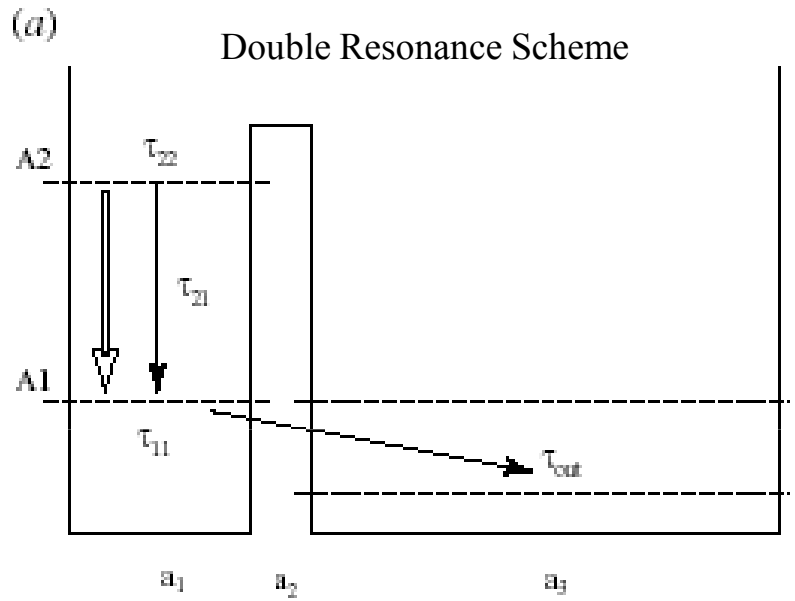

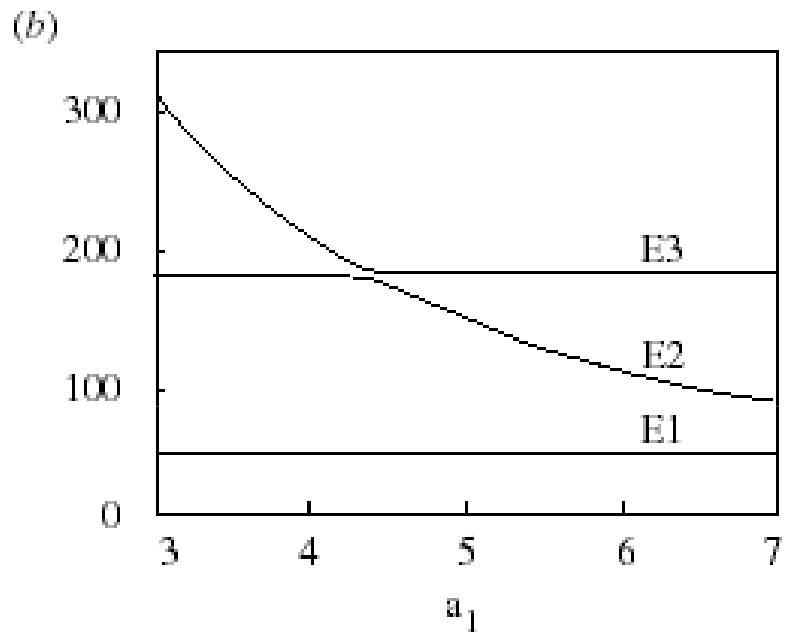

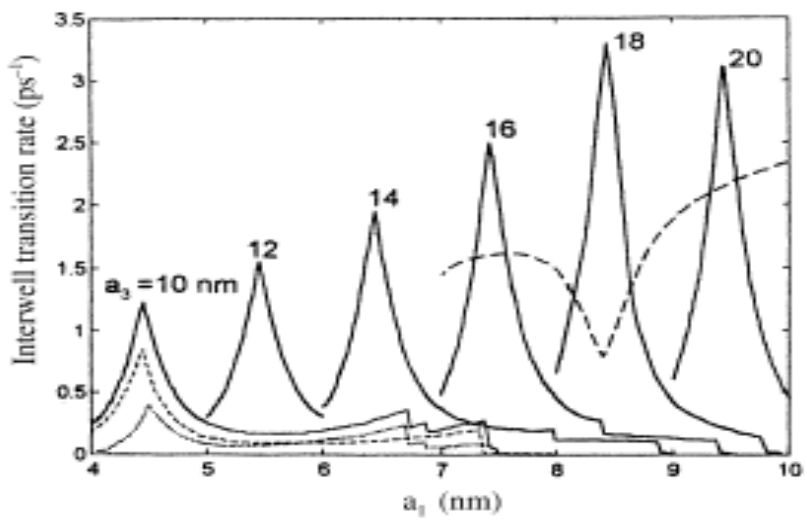

Michael A. Stroscio, Mikhail V. Kisin, Gregory Belenky, and Serge Luryi, Phonon Enhanced Inverse Population in Asymmetric Double Quantum Wells, Applied Physics Letters, 75, 3258 (1999).

Interface-Phonon-Assisted Processes

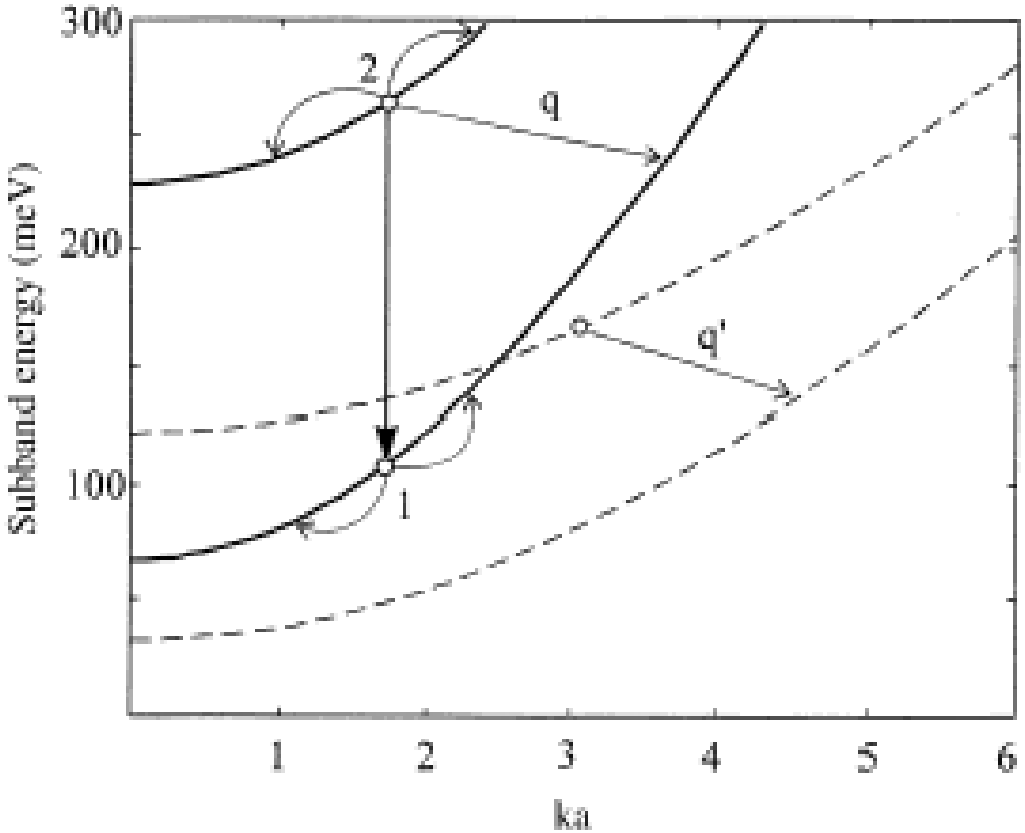

Figure 10.7. Energy dispersion curves for 60-ångstrom-wide (solid lines) and 100-ångstrom-wide (broken lines) $Al_{0.3}Ga_{0.7}As/GaAs/Al_{0.3}Ga_{0.7}As$ quantum wells. Typical intersubband and intrasubband transitions are shown for both quantum wells. The energy gap for the GaAs well, E_g(GaAs), is taken as 1.4 eV and the ratio of the effective mass to the electron mass is taken as 0.067 for GaAs. From Kisin *et al.* (1997), American Institute of Physics, with permission.

References 4 and 5:

M. Kisin, M. Stroscio, V. Gorfinkel, G. Belenky and S. Luryi, Influence of Complex Phonon Spectrum of Heterostructure on Gain Lineshape in Quantun Cascade Laser (QCL), Optical Society of America, Technical Digest Series, Volume 11, 425 (1997).

Mikhail V. Kisin, Vera B. Gorfinkel, Michael A. Stroscio, Gregory Belenky, and Serge Luryi, Influence of Complex Phonon Spectra on Intersubband Optical Gain, J. Appl. Phys., 82, 2031 (1997).

----- 10 nm
____ 6 nm

AlGaAs-GaAs-AlGaAs
x = 0.3

Interface-Phonon-Assisted Processes, Con't

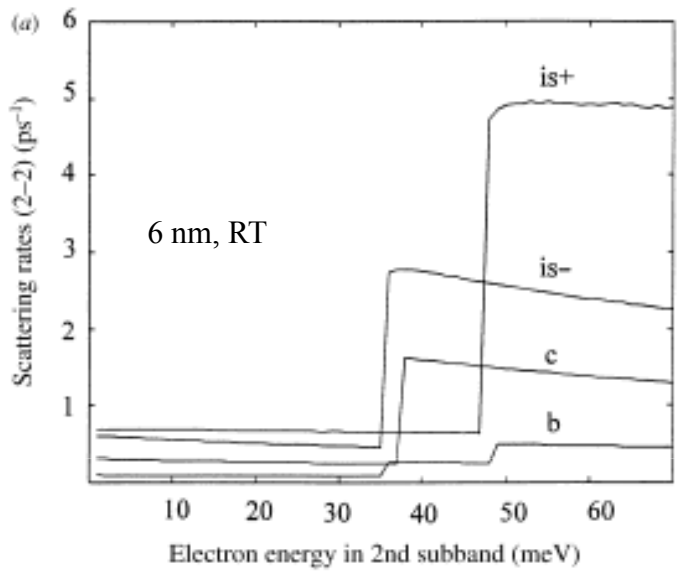

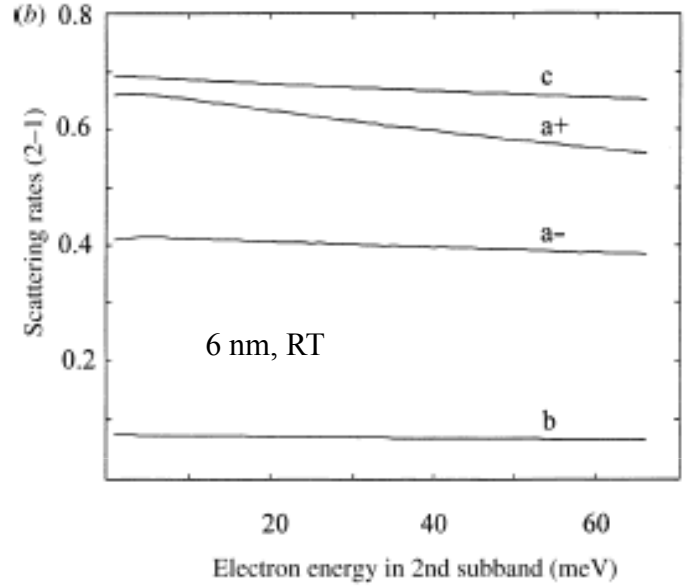

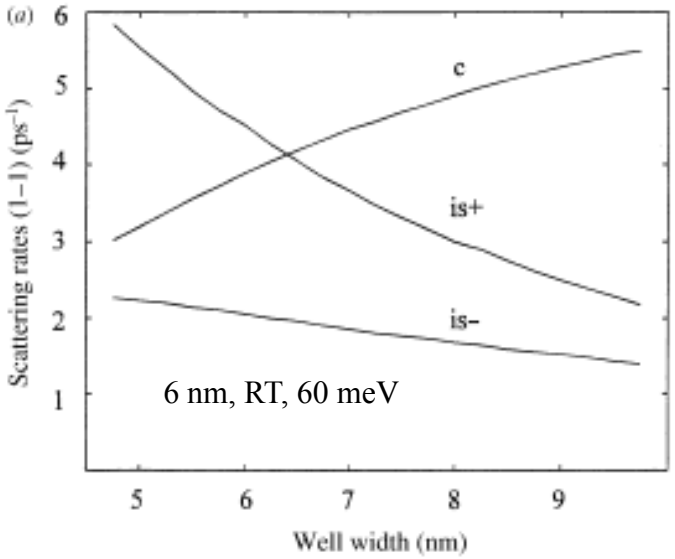

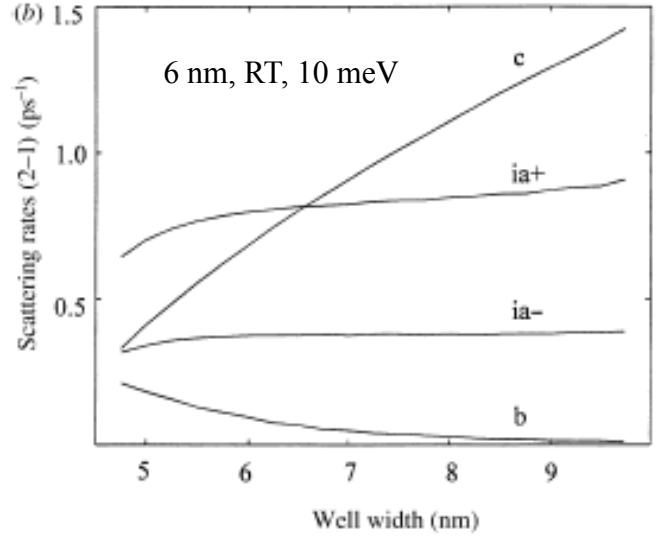

Interface-Phonon-Assisted Processes, Con't

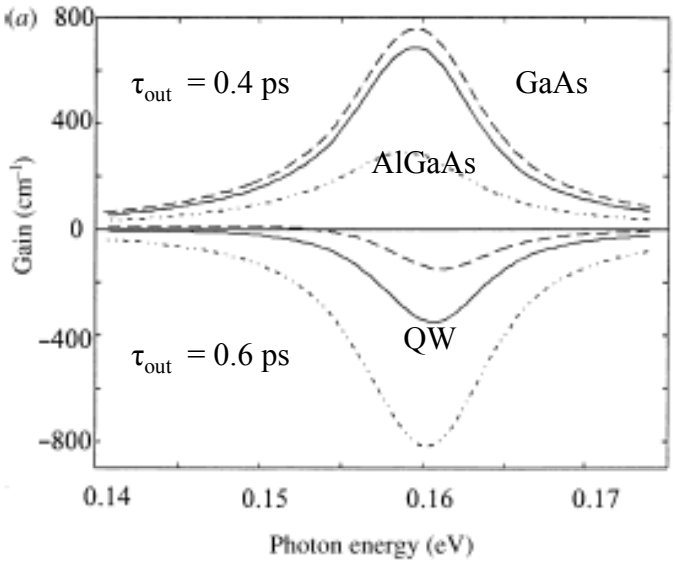

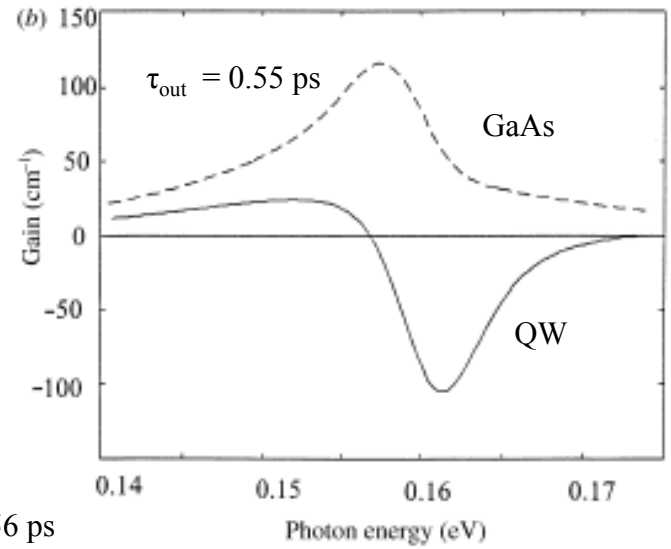

τ_{1-2} = 0.56 ps

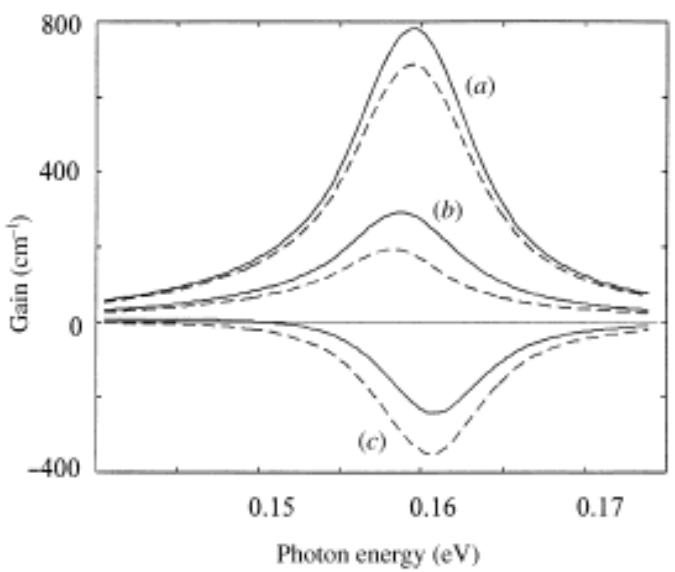

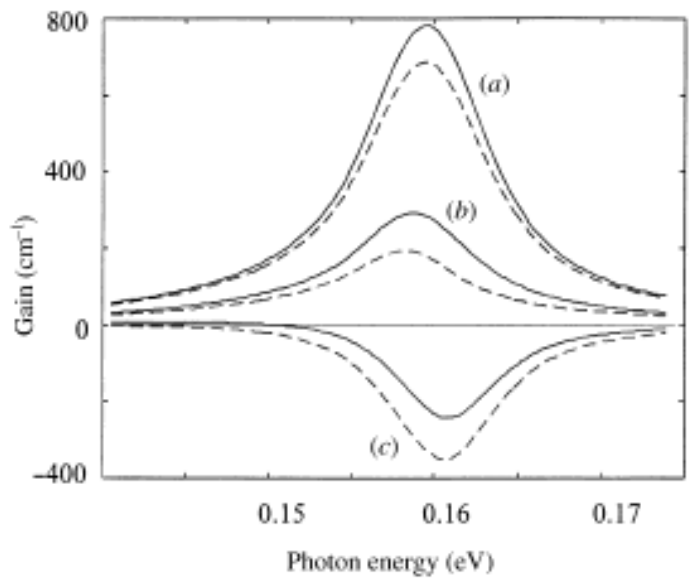

--- all modes
__ w/o barrier modes
A - 0.4 ps,
B - 0.5 ps,
C - 0.6 ps

Phonon Engineering: Some Key Techniques

- Dimensional Confinement and Boundary Effects Cause Plane Wave Phonons (Bulk Phonons) to by Replaced by Set of Modes --- Same as Putting Electromagnetic Wave in a Waveguide

- Bulk modes $\rightarrow$ Confined modes, plus interface modes, plus half-space modes with new energies, and spatial profiles.

SINCE CARRIER INTERACTIONS MUST CONSERVE ENERGY AND MOMENTUM HAVING NEW PHONON ENERGIES LEADS TO WAYS TO MODIFY CARRIER SCATTERING AND TRANSPORT…

Phonon Engineering: Some Key Techniques

EXPLOITING THE FACT THAT NEW ENERGIES LEADS TO WAYS TO MODIFY CARRIER SCATTERING AND TRANSPORT ---

•Phonon assisted transitions → Example: use to enhance population inversions in Quantum Cascade Lasers, Type-II Lasers, etc.

•Change phase space to modify interactions → In devices based on quantum wells, quantum wires, and quantum dots reduces the set of phonon momenta and energies allowed in transitions --- Example: Phase-space reductions in CNTs lead to enhanced carrier mobilities

• Modify materials to change phonons and thus interactions → Examples: (a) Form metal-semiconductor inteface to eliminate selected interface modes; (b) Reduce carrier-phonon interactions through the design of $In_xGa_{-x}N$-based structures exhibiting one mode behavior

•Modify phonon lifetimes (by arranging for different anharmonic terms) and phonon speeds (by modifying dispersion relations)→ Reduce bottleneck effects; modify thermal transport

• Generate coherent phonons using Cerenkov effect (as an example) to amplify phonon effects

Some areas where phonon engineering has clear payoff:

improved gain in semiconductor lasers (especially lasers with narrow quantum wells like quantum cascade lasers),

enhance gain in Sb-lased lasers,

coherent phonon sources for non-charge-based binary switches and devices,

increasing carrier mobilities in CNTs,

improving CNT-based IR detectors based on understand phonon-assisted non-radiative recombination,

improving III-nitride-based device performance,

phonon engineering to modify thermal conductivity.

Interface-Phonon-Assisted Processes: Enhanced Population Inversion

United States Patent 6,819,696 Belenky, Dutta, Kisin, Luryi, and Stroscio. November 16, 2004
United States Patent 7,310,361 Belenky, Dutta, Kisin, Luryi, and Stroscio. December 18, 2007

Intersubband semiconductor lasers with enhanced subband depopulation rate

Abstract
Intersubband semiconductor lasers (ISLs) are of great interest for mid-infrared (2-20 micron) device applications. These semiconductor devices have a wide range of applications from pollution detection and industrial monitoring to military functions. ISLs have generally encountered several problems which include slow intrawell intersubband relaxation times due to the large momentum transfer and small wave-function overlap of the initial and final electron states in interwell transitions. Overall, the ISL's of the prior art are subject to weak intersubband population inversion. The semiconductor device of the present invention provides optimal intersubband population inversion by providing a double quantum well active region in the semiconductor device. This region allows for small momentum transfer in the intersubband electron-phonon resonance with the substantial wave-function overlap characteristic of the intersubband scattering.
Inventors: **Belenky; Gregory** (Port Jefferson, NY); **Dutta; Mitra** (Wilmette, IL); **Kisin; Mikhail** (Lake Grove, NY); **Luryi; Serge** (Setanket, NY); **Stroscio; Michael** (Wilmette, IL) Assignee: **The United States of America as represented by the Secretary of the Army** (Washington, DC) Appl. No.: **957531** Filed: **September 21, 2001**

Resonant phonon-assisted depopulation in type-I and type-II intersubband laser heterostructures

M. V. Kisin[1], M. A. Stroscio[2], G. Belenky[1], and S. Luryi[1]

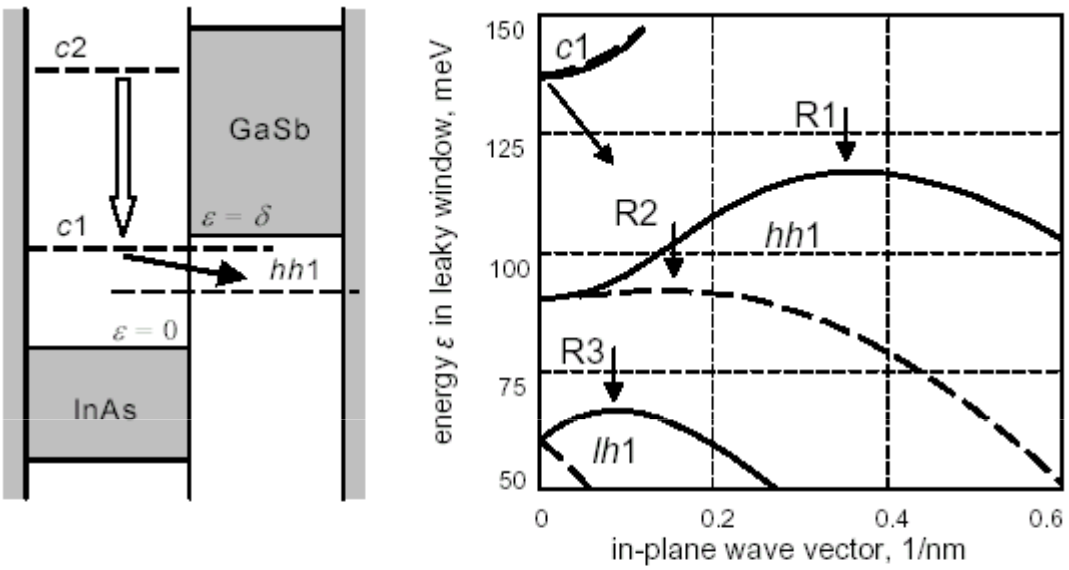

Figure 1. Left: schematic band diagram of an asymmetric InAs/GaSb DQW modeling an active region of intersubband type-II cascade laser. Black arrow depicts the interband LO-phonon assisted depopulation process. Right: subband splitting in the upper part of the leaky window δ. Short vertical arrows indicate the positions of the Van Hove singularities.

In conclusion, we show that in type-II intersubband laser heterostructures the interband LO-phonon-assisted scattering can be used as an efficient complementary process for the fast depopulation of the lower lasing states.

Inst. Phys. Conf. Ser. No 174: Section 5
Paper presented at 29th Int. Symp. Compound Semiconductors, Lausanne, Switzerland, 7-10 October 2002
©2003 IOP Publishing Ltd

Phonon-Assisted Transitions in Heterostructure Lasers

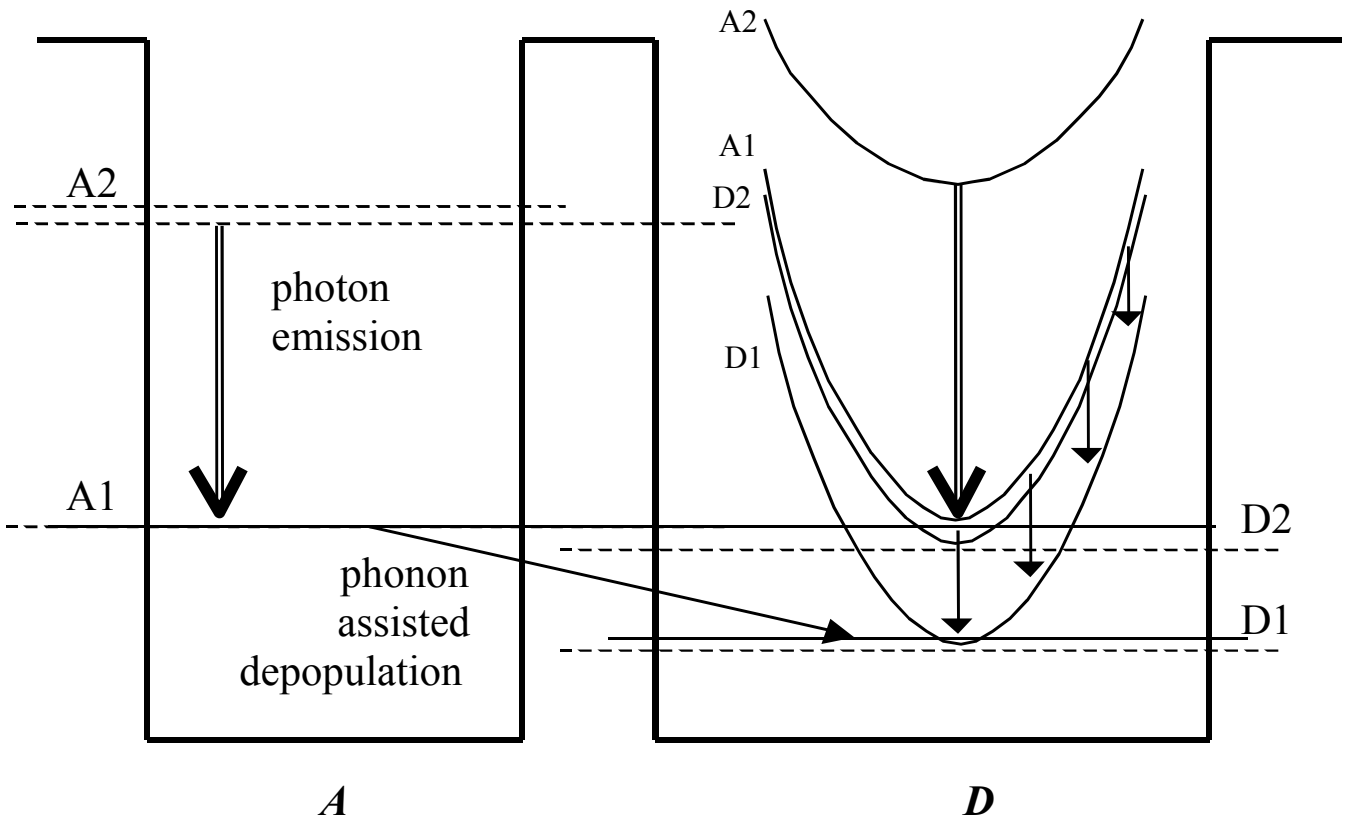

Interface-Phonon-Assisted Processes: Double Resonance Process

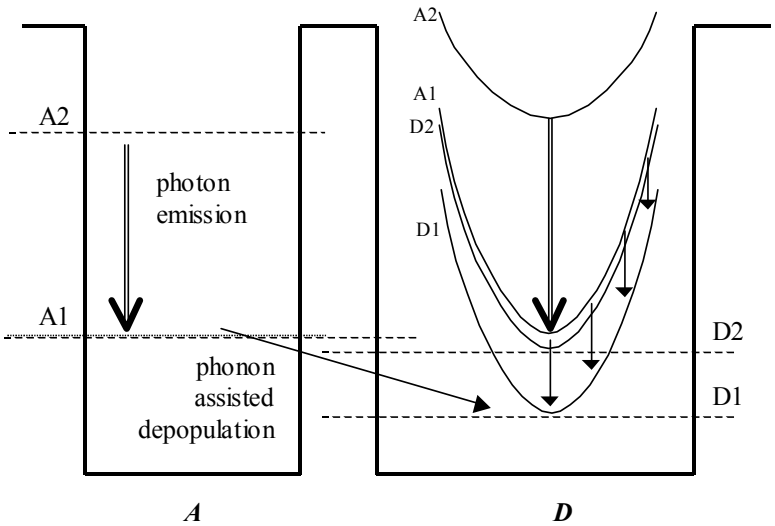

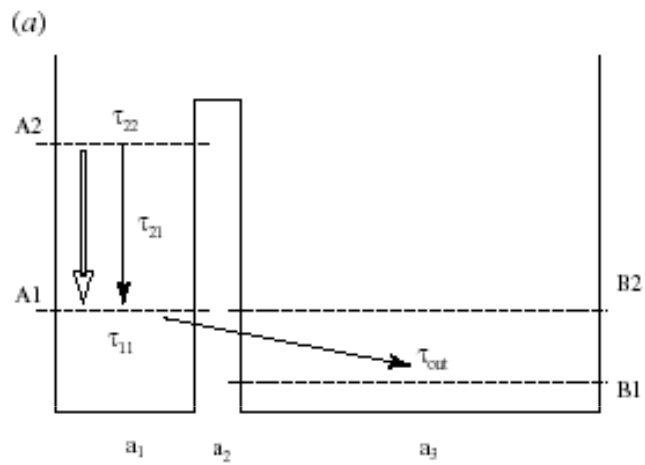

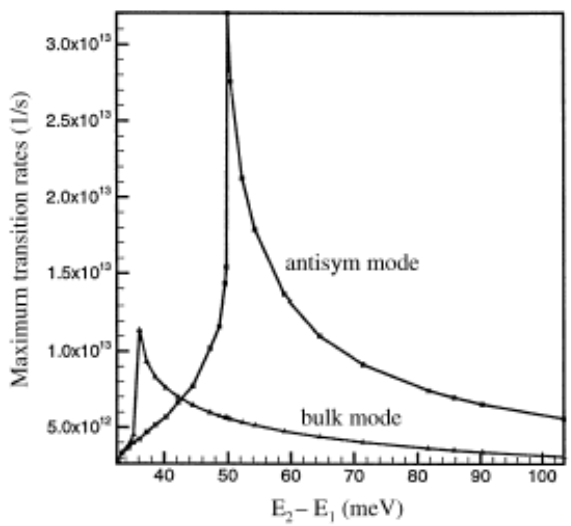

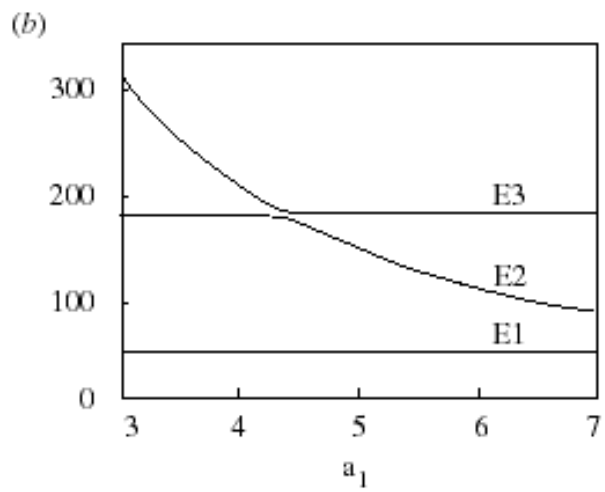

References 1-9

Interface-Phonon-Assisted Processes

1. M. Dutta, H. L. Grubin, G. J. Iafrate, K. W. Kim and M. A. Stroscio, Metal-Encapsulated Quantum Wire for Enhanced Charge Transport, CECOM Docket Number 4734, disclosed September 1991; filed September 15, 1992 (Serial No. 07/945040); Patent No. 5,264,711 issued November 23, 1993.

2. Michael A. Stroscio, Interface-Phonon--Assisted Transitions in Quantum Well Lasers, JAP, 80, 6864 (1996). --- **Strong interaction of interface modes first pointed out.**

3. SeGi Yu, K. W. Kim, Michael A. Stroscio, G. J. Iafrate, J.-P. Sun, and G. I. Haddad, Transfer Matrix Technique for Interface Optical Phonon Modes in Multiple Quantum Well Systems, JAP, 82 3363 (1997).

4. M. Kisin, M. Stroscio, V. Gorfinkel, G. Belenky and S. Luryi, Influence of Complex Phonon Spectrum of Heterostructure on Gain Lineshape in Quantun Cascade Laser (QCL), Optical Society of America, Technical Digest Series, Volume 11, 425 (1997).

5. Mikhail V. Kisin, Vera B. Gorfinkel, Michael A. Stroscio, Gregory Belenky, and Serge Luryi, Influence of Complex Phonon Spectra on Intersubband Optical Gain, J. Appl. Phys., 82, 2031 (1997).

6. Mitra Dutta and Michael A. Stroscio, Comment on Energy Level Schemes for Far-Infrared Quantum Well Lasers, Appl. Phys. Lett., 74, 2555 (1999).

7. Michael A. Stroscio, Mikhail V. Kisin, Gregory Belenky, and Serge Luryi, Phonon Enhanced Inverse Population in Asymmetric Double Quantum Wells, Applied Physics Letters, 75, 3258 (1999).

8. J. P. Sun, G. I. Haddad, Mitra Dutta, and Michael A. Stroscio, Quantum Well Intersubband Lasers, International Journal of High Speed Electronic Systems, 9, 281 (1998).

9. Gregory Belenky, Mitra Dutta, Mikhail Kisin, Serge Luryi, and Michael Stroscio, Intersubband Semiconductor Lasers with Enhanced Subband Depopulation Rate, invention disclosure filed November 2001; U.S. Patent No. 6,819,696, November 16, 2004.

Interface-Phonon-Assisted Processes: Applications

1. M. Dutta, H. L. Grubin, G. J. Iafrate, K. W. Kim and M. A. Stroscio, Metal-Encapsulated Quantum Wire for Enhanced Charge Transport, CECOM Docket Number 4734, disclosed September 1991; filed September 15, 1992 (Serial No. 07/945040); Patent No. 5,264,711 issued November 23, 1993.
2. Michael A. Stroscio, Interface-Phonon--Assisted Transitions in Quantum Well Lasers, JAP, 80, 6864 (1996).
5. Mikhail V. Kisin, Vera B. Gorfinkel, Michael A. Stroscio, Gregory Belenky, and Serge Luryi, Influence of Complex Phonon Spectra on Intersubband Optical Gain, J. Appl. Phys., 82, 2031 (1997).
6. Mitra Dutta and Michael A. Stroscio, Comment on Energy Level Schemes for Far-Infrared Quantum Well Lasers, Appl. Phys. Lett., 74, 2555 (1999).
9. Gregory Belenky, Mitra Dutta, Mikhail Kisin, Serge Luryi, and Michael Stroscio, Intersubband Semiconductor Lasers with Enhanced Subband Depopulation Rate, invention disclosure filed November 2001;
U.S. Patent No. 6,819,696, November 16, 2004.

B. S. Williams, B. Xu, Q. Hu, Narrow-linewidth Terahertz Emission from Three-level Systems, APL, 75, 2927 (1999); Refs. 2 and 5.

V. M. Menon, L. R. Ram-Mohan, W. D. Goodhue, A. J. Gatesman, A. S. Karakashian, "Role of Interface Phonons in Quantum Cascade Terahertz Emitters," Physica B, 316-317, 212-215 (2002); Ref. 6 and Yu, Kim, Stroscio, Iafrate, Sun, and Haddad, JAP, 82, 3363 (1997).

V. Spagnolo, G. Scamarcio, M. Troccoli, F, Capasso, C. Gmachl, A. M. Sergent, A. L. Hutcheson, D. L. Sivco, and A. Y. Cho, Nonequilibrium Optical Phonon Generation by Steady State Electron Transport in Quantum-Cascade Lasers, APL, 80, 4303-4305 (2002); Ref. 2 and Komirenko papers on nonequilibrium phonons (APL, 77, 4178 (2000) and PRB, 63, 165308, (2000).

Mariano Troccoli, Alexey Belyanin, Federico Capasso, Ertugrul Cubukcu, Deborah L. Sivco, and Alfred Y. Cho, Raman Injection Laser, Nature, 433, 845-848 (2005).

Implemented in QCL-like Heterostructure

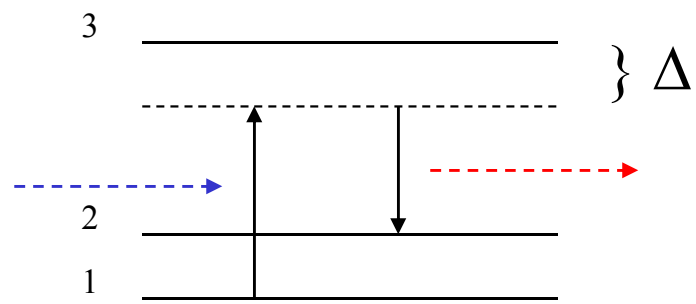

Interface-Phonon-Assisted Processes: Enhanced Population Inversion

United States Patent 6,819,696 Belenky, Dutta, Kisin, Luryi, and Stroscio. November 16, 2004
United States Patent 7,310,361 Belenky, Dutta, Kisin, Luryi, and Stroscio. December 18, 2007

Intersubband semiconductor lasers with enhanced subband depopulation rate

Abstract
Intersubband semiconductor lasers (ISLs) are of great interest for mid-infrared (2-20 micron) device applications. These semiconductor devices have a wide range of applications from pollution detection and industrial monitoring to military functions. ISLs have generally encountered several problems which include slow intrawell intersubband relaxation times due to the large momentum transfer and small wave-function overlap of the initial and final electron states in interwell transitions. Overall, the ISL's of the prior art are subject to weak intersubband population inversion. The semiconductor device of the present invention provides optimal intersubband population inversion by providing a double quantum well active region in the semiconductor device. This region allows for small momentum transfer in the intersubband electron-phonon resonance with the substantial wave-function overlap characteristic of the intersubband scattering.
Inventors: **Belenky; Gregory** (Port Jefferson, NY); **Dutta; Mitra** (Wilmette, IL); **Kisin; Mikhail** (Lake Grove, NY); **Luryi; Serge** (Setanket, NY); **Stroscio; Michael** (Wilmette, IL) Assignee: **The United States of America as represented by the Secretary of the Army** (Washington, DC) Appl. No.: **957531** Filed: **September 21, 2001**

Phonon-Assisted Processes: Applications to Enhanced Heterostructure Laser Performance

IMPROVEMENTS IN HETERSTRUCTURE LASER PERFORMANCE

- Population Inversions Enhanced by Over an Order of Magnitude
- Gain-length Reduced → Greater Coherence and Compact Devices
- Improved Carrier Injection → Reduced Chirp

These improvements result primarily because in optoelectronic devices energy selectivity matters and it is accordingly possible to select one engineered phonon mode to precisely engineering/control the desired interactions/parameters.

Phonon Engineering in CNTs to Optimize

- Carrier Mobilities
- IR Detectors

Enhanced Mobilities due to Phonon Bottlenecks

Intravalley Intersubband 2 ⟷ 1 ⟶ n=1

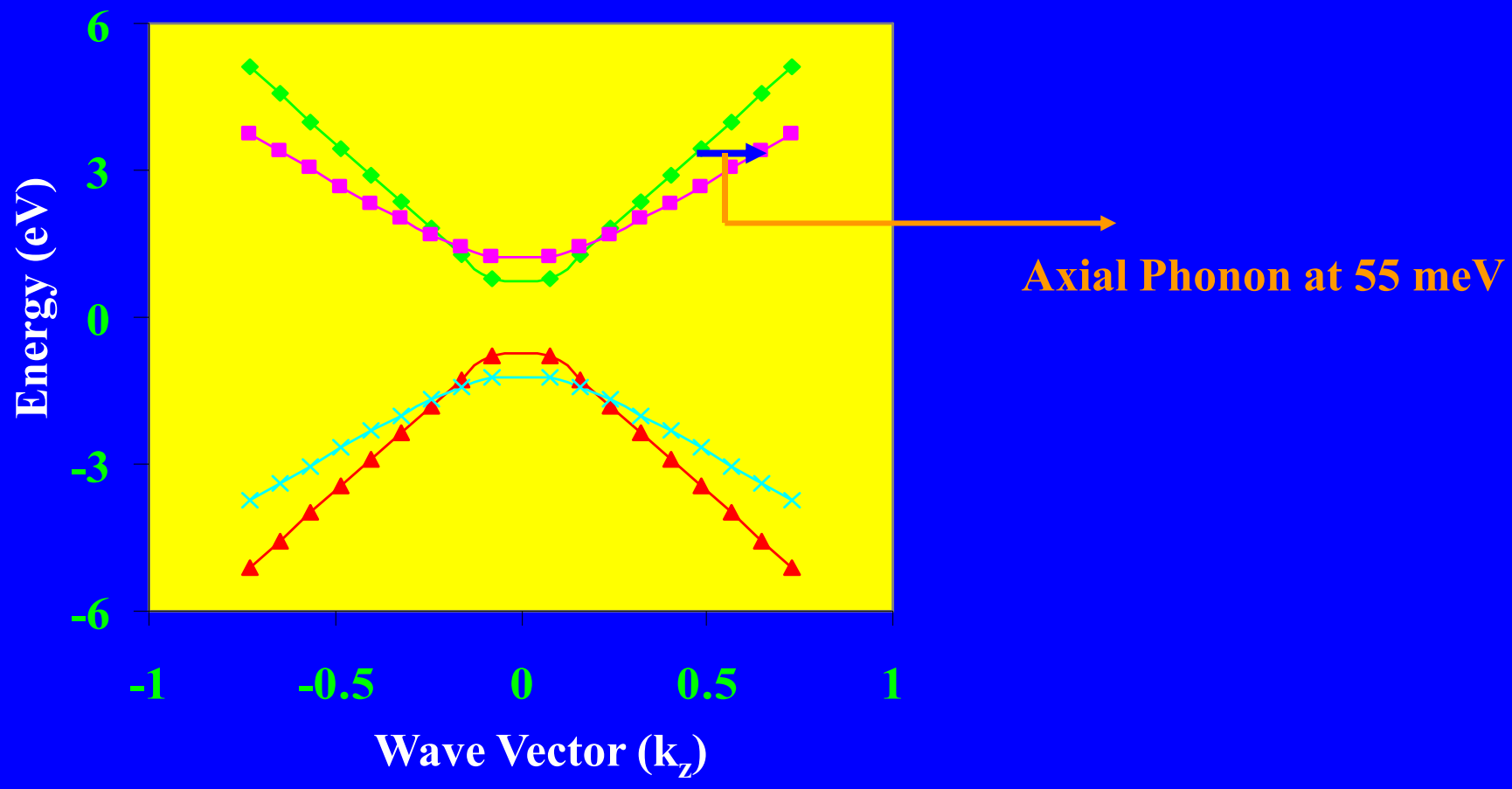

Bandgap of Zigzag Nanotube as a Function of Circumference, L/a

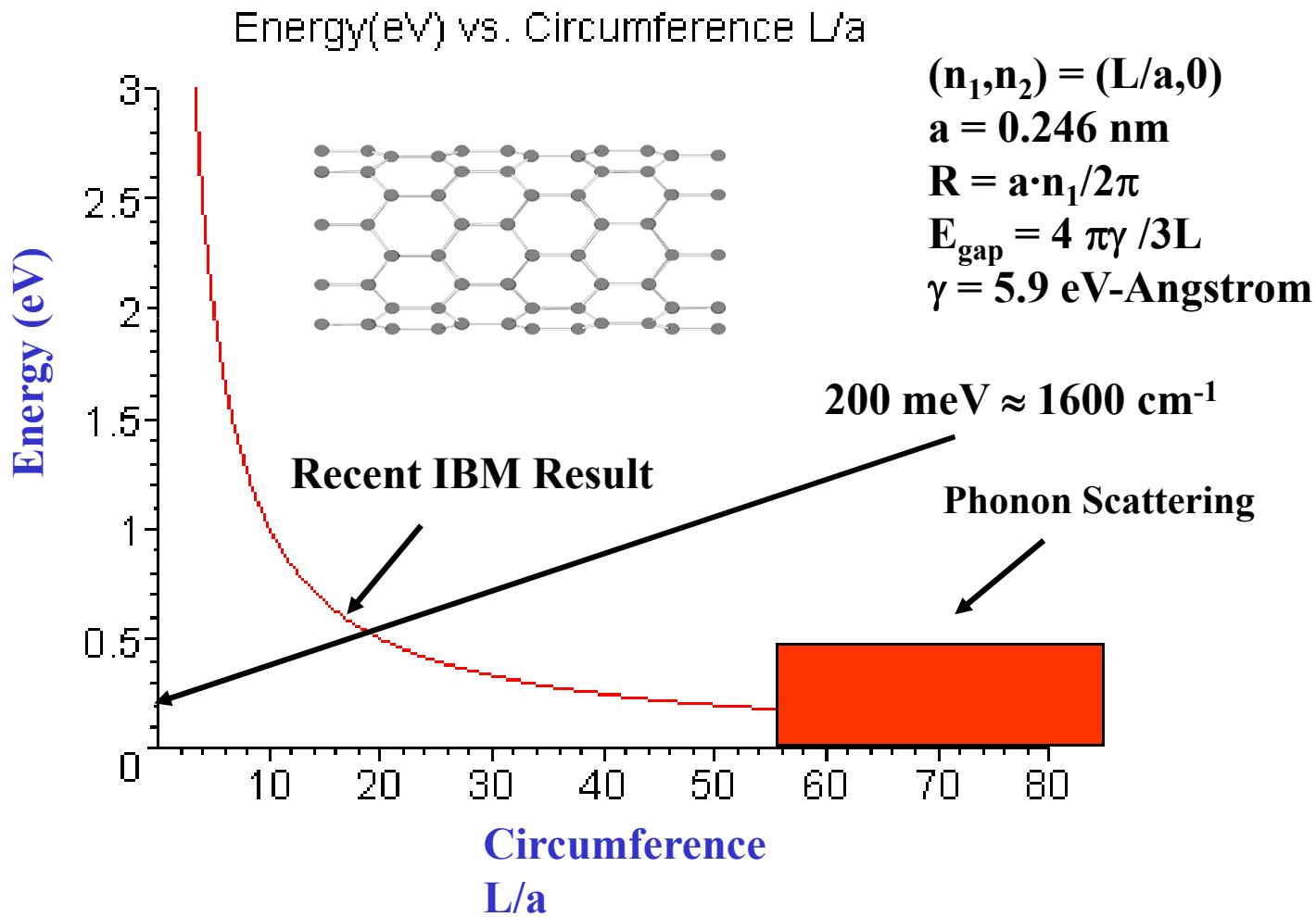

$(n_1,n_2) = (L/a,0)$

$a = 0.246$ nm

$R = a \cdot n_1/2\pi$

$E_{gap} = 4\pi\gamma/3L$

$\gamma = 5.9$ eV-Angstrom

Phonon Engineering to Modify Thermal Conductivity

PHYSICAL REVIEW B VOLUME 5, NUMBER 12 15 JUNE 1972

Lattice Dynamics of Pyrolytic Graphite*

R. Nicklow, N. Wakabayashi, and H. G. Smith
Solid State Division, Oak Ridge National Laboratory, Oak Ridge, Tennessee 37830
(Received 3 December 1971)

v_{LA}
$(2.36 \times 10^4 \text{ m/s})$

v_{TA}
$(1.59 \times 10^4 \text{ m/s})$

$$\frac{2}{\langle v \rangle^2} = \frac{1}{\langle v_{LA} \rangle^2} + \frac{1}{\langle v_{TA} \rangle^2}$$

$$v = 1.86 \times 10^4 \text{ m/s}$$

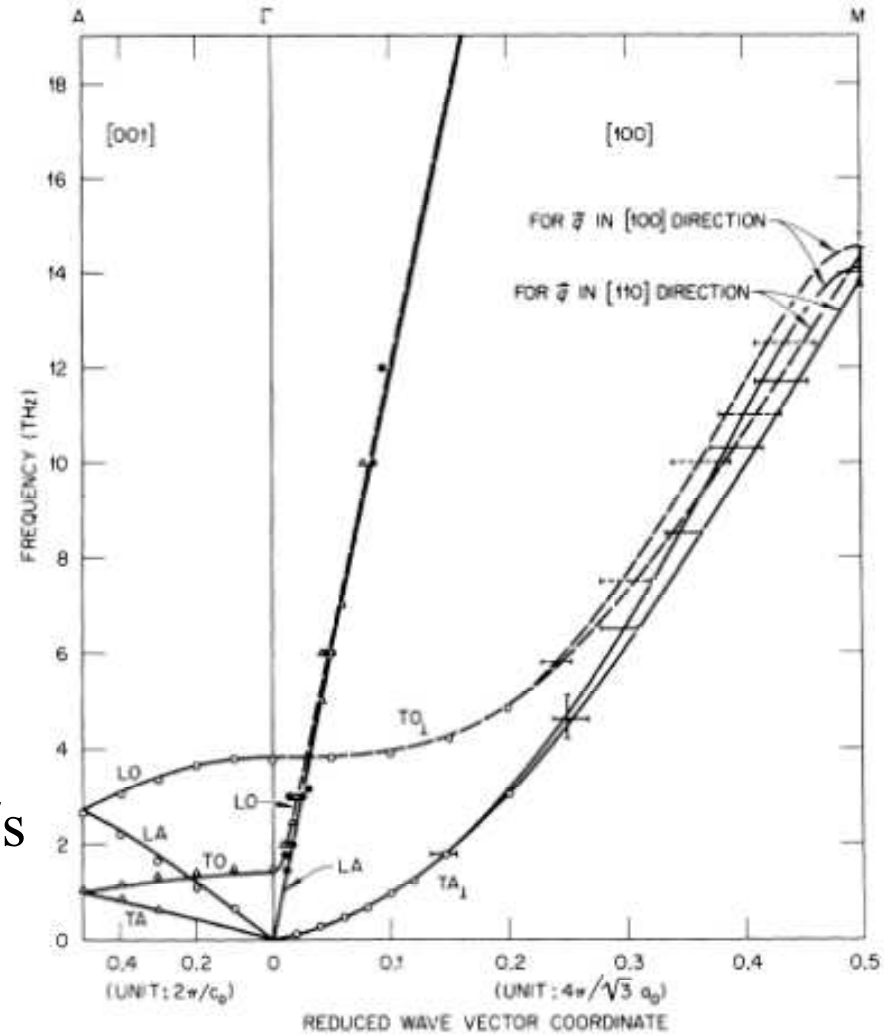

FIG. 6. Phonon frequencies measured for pyrolytic graphite. All measurements for $\vec{q}$ in the basal plane have been plotted with $\vec{q}$ expressed in units appropriate for the [100] direction. The lines shown represent calculations with the fourth-nearest-neighbor AS model discussed in the text. For the $TA_\perp$ and $TO_\perp$ branches calculations for $\vec{q}$ in both the [100] and [110] directions are shown to illustrate the approximate isotropy of these branches.

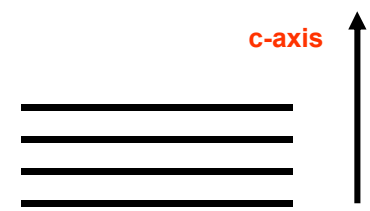

2D intrinsic thermal conductivity of graphite

$$\lambda_i(T) = \frac{1}{2}\int_{f_c}^{f_d} C_2(f)\, v l_i(f,T)\, df$$

$$l_i(f,T) = \frac{Mv^3 f_d}{4pg^2 kTf^2}$$

$$C_2(f) = \frac{4kf}{a^3 f_d^{\,2}}$$

$$f_d = 4.6\times10^{13}\ \text{Hz}$$

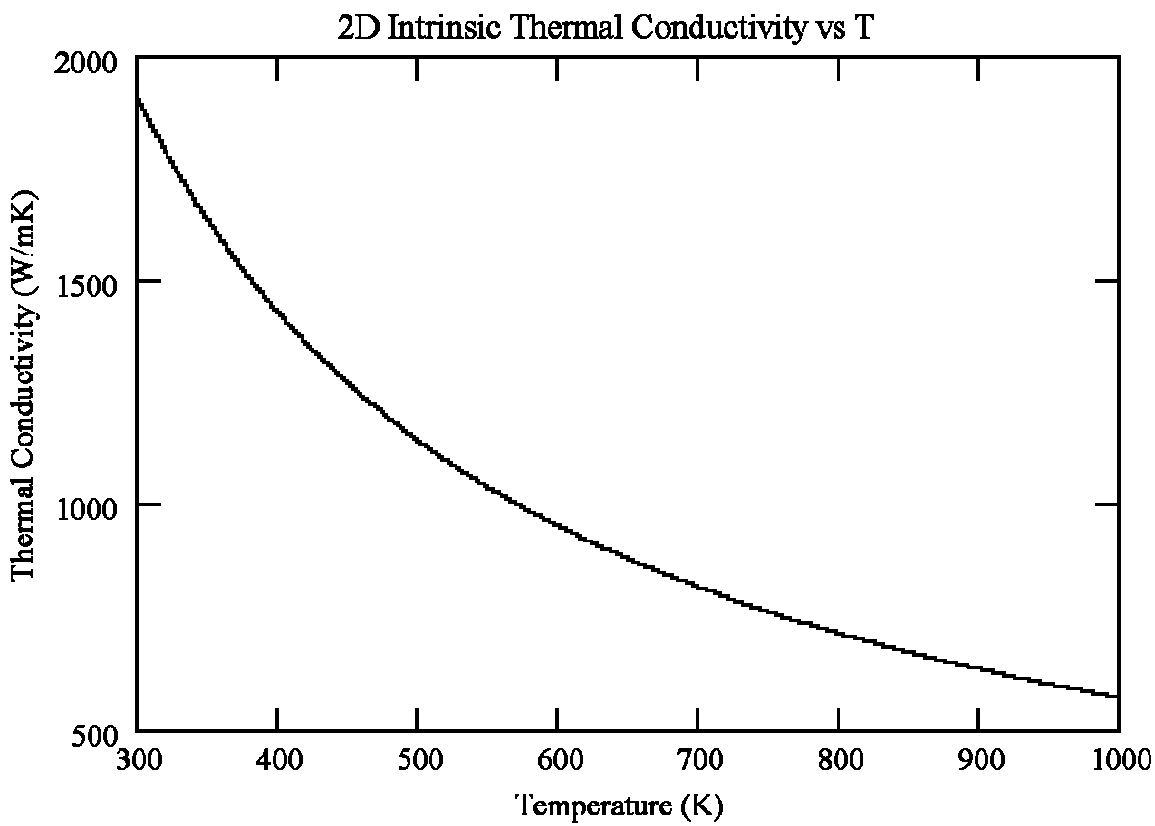

Two-dimensional intrinsic thermal conductivity of graphite as a function of temperature.

P. G. Klemens, “Graphite, Graphene and Carbon Nanotubes”, *Thermal Conductivity 26*, p. 48

Effective average point defect concentration

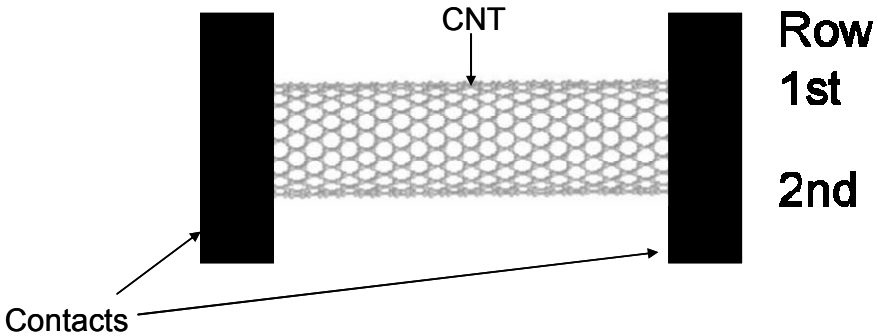

$$c = \frac{2}{2Nn} = \frac{1.5}{10 \times \left(\frac{l_n}{d} + 1\right)}$$

N: number of circumferential atoms
n: number of rows
l_n: length of CNT
d: distance between 2 nearest atoms

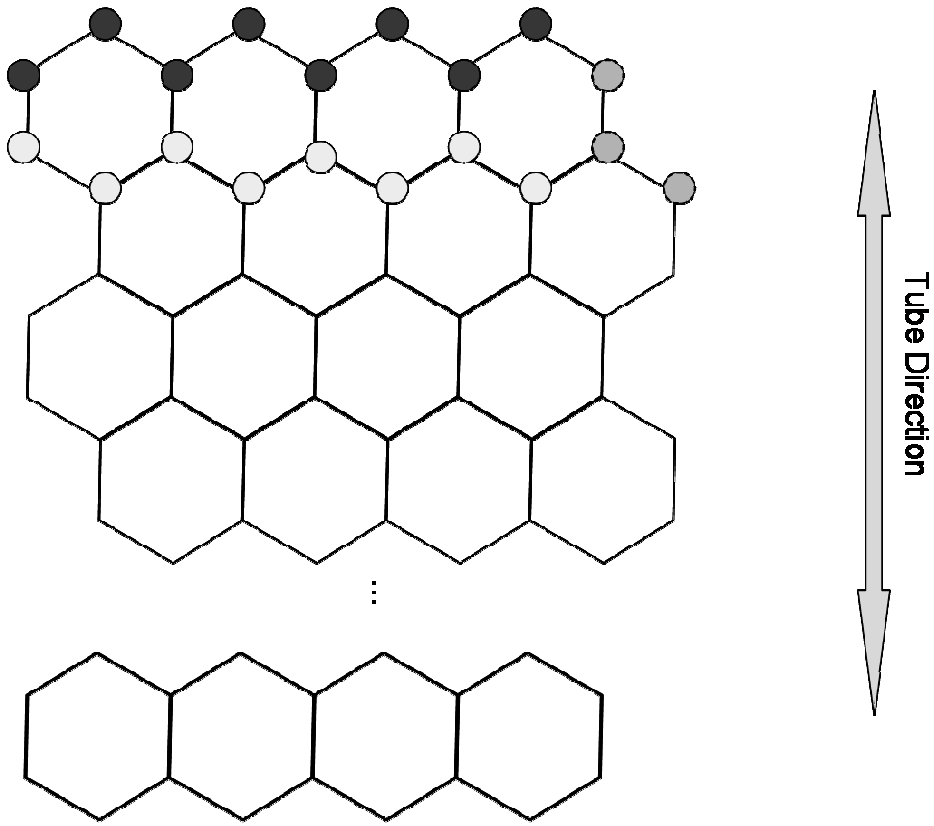

Ke Sun et al.

Effective average point defect concentration

Ke Sun et al.

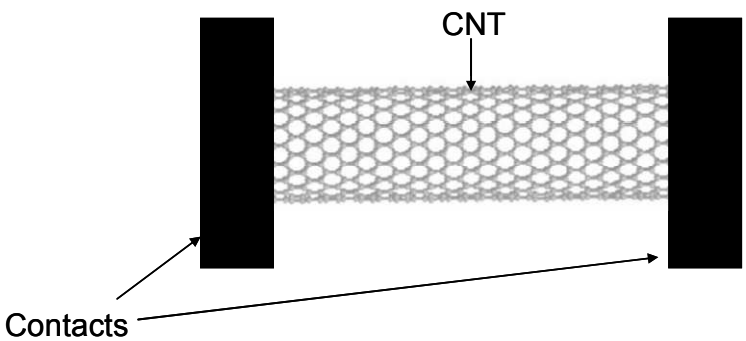

Since for a tube of 1 row, its length is 0.5d, where d is the length of the side of the hexagon equal to 0.142 nm, and for n rows, the tube length is

$$l_n = 0.5d + (n-1)\times 1.5d\ ,$$

the number of rows is thus

$$n = \frac{\left(\frac{l_n}{d}+1\right)}{1.5}$$

and the total number of atoms in the carbon nanotube is 2Nn. With one defect at each end of the tube the average point defect concentration is

$$c = \frac{2}{2Nn} = \frac{1.5}{10\times\left(\frac{l_n}{d}+1\right)}.$$

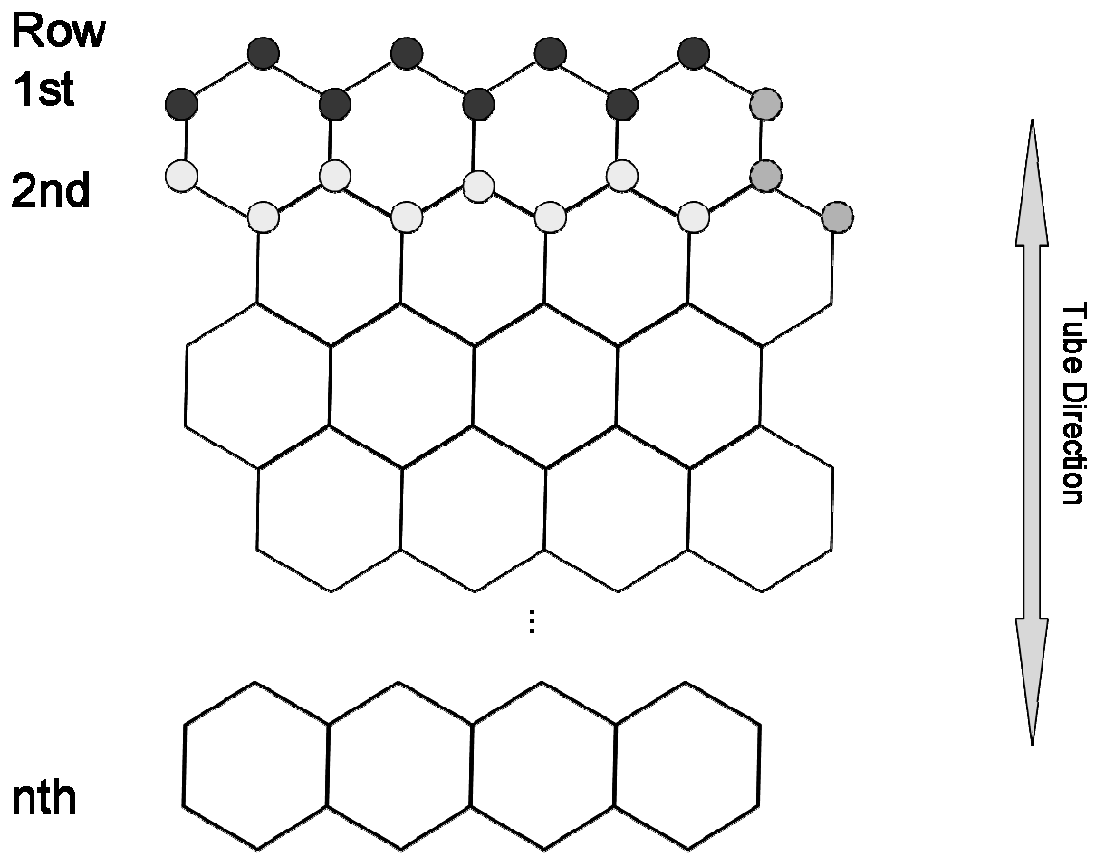

N: number of circumferential atoms
n: number of rows
l_n: length of CNT
d: distance between 2 nearest atoms

End effects of point defects

$$\frac{1}{l_p(f)} = Af^3 = c\left(\frac{\Delta M}{M}\right)^2 4\pi^2\left[vf_d^2\right]^{-1} f^3$$

$$\frac{1}{l} = \frac{1}{l_i} + \frac{1}{l_p}$$

$$\lambda_p(T) = \frac{1}{2}\int_{f_c}^{f_d} C_2(f)\, vl(f,T)\, df$$

$$= \frac{2.34\times10^5}{T}\left[\ln\left(\frac{f_d}{f_c}\right) - \ln\left(\frac{1+\frac{f_d}{f_0}}{1+\frac{f_c}{f_0}}\right)\right]$$

$$f_0 = 2.556\times10^{-6} f_d T\left[\frac{1.35}{\frac{l_n}{d}+1}\right]^{-1}$$

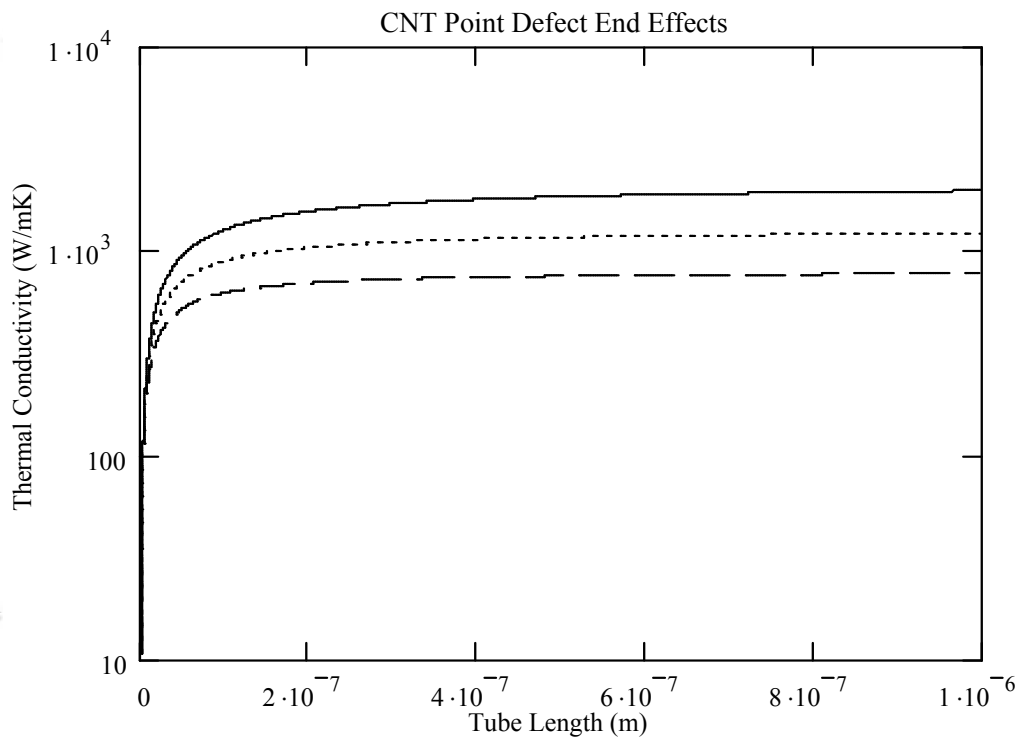

End effects of point defects on CNT thermal conductivity:

solid line is at 300 K,
dotted line is at 500 K
dashed line is at 800 K

Ke Sun et al.

Compare point defect scattering and boundary scattering

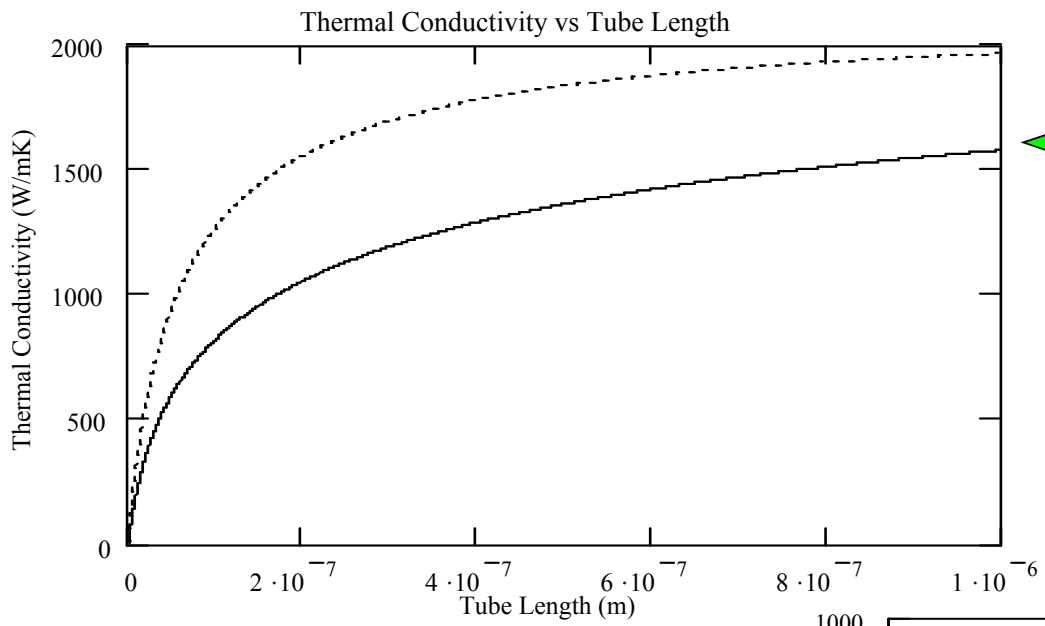

Thermal conductivity as a function of CNT tube length at 300 K.

Thermal conductivity as a function of temperature for a single-wall CNT of about 21.2 nm in length: - solid line is for boundary scattering

- dotted line is for point-defect scattering.

$$\lambda_B(T) = \frac{1}{2}\int_{f_c}^{f_d} C_2(f)\, v l(f,T)\, df$$

$$= \frac{1.17\times 10^5}{T}\ln\left(\frac{f_d^2 + f_B^2}{f_c^2 + f_B^2}\right)$$

$$\frac{1}{l} = \frac{1}{l_i} + \frac{1}{l_B} \text{ and } f_B^2 = \frac{M v^3 f_d v}{4\pi\gamma^2 k T l_B}$$

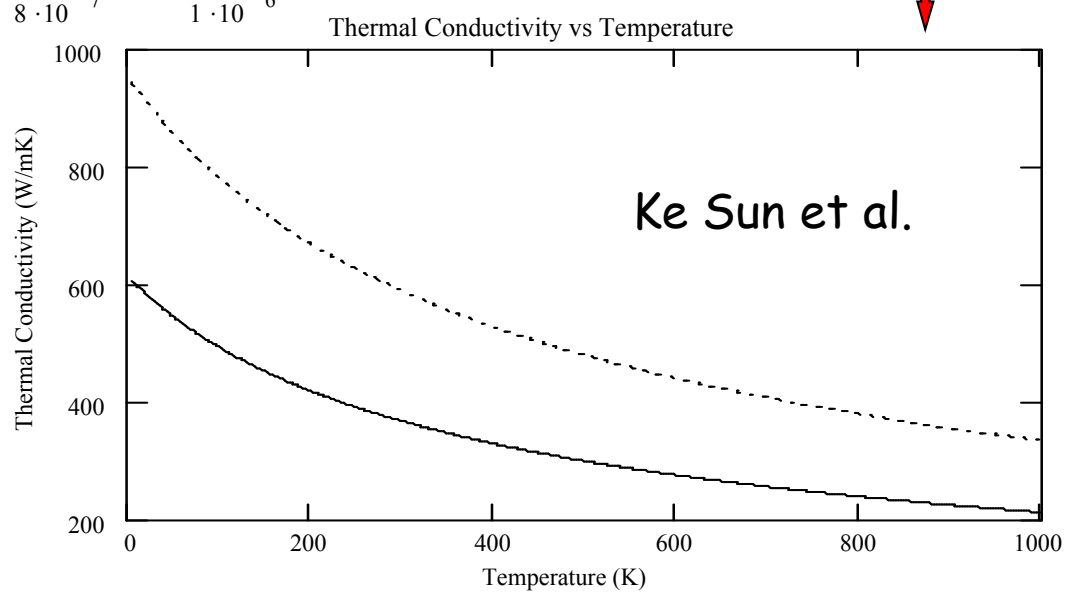

Thermoelectric figure of merit

Ke Sun et al.

$$ZT = S^2 s\, T / l$$

S is the Seebeck coefficient, σ is the electric conductivity, T is the absolute temperature and λ is the thermal conductivity

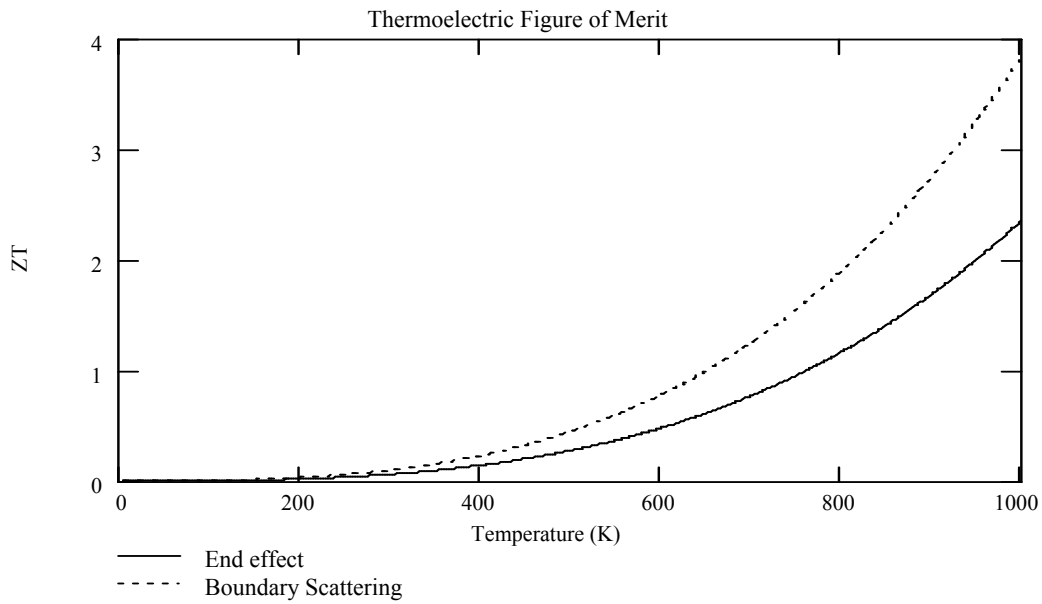

Thermoelectric figure of merit as a function of temperature for a single-wall CNT of about 4.1 nm in length.

High *ZT* values achieved in other systems include $AgPb_mSbTe_{2+m}$ reported to exhibit a *ZT* of ~2.2 at 800 K. *ZT* values of 2.0 at 300 K have been obtained for PbSnSeTe alloy materials and ~0.8 for the material $CsBi_4Te_6$ produced at 225 K

Summary: Thermal Effects

- Studied 2D graphite intrinsic thermal conductivity as a function of temperature.
- Included effects of point defect scattering and boundary scattering
- High ZT values are obtained for CNTs of submicron lengths

Graphene: Confined Phonons

Ribbons
Quantum Dots

Jun Qian et al.

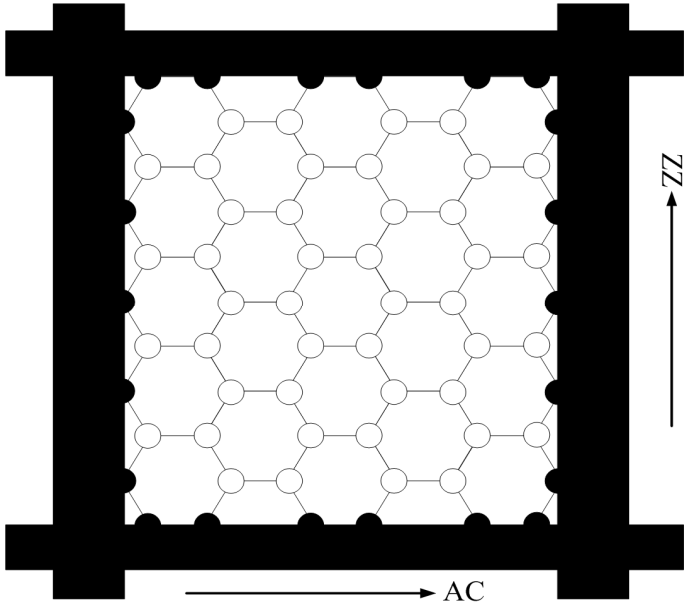

Confined Phonons in 2D Graphene Sheet

$$\ddot{U} = \hat{\Delta}^{opt} U, \qquad U = u_A - u_B = \begin{pmatrix} u \\ v \\ w \end{pmatrix}$$

Jun Qian et al.

$$-\hat{\Delta}_{2DG}^{opt} = \omega_{TO}^2 + \frac{\beta_T^2 - \beta_L^2}{2} J_Z^2 \nabla_\perp^2 + \frac{\beta_T^2 + \beta_L^2}{2}\left(\nabla_-^2 J_+^2 + \nabla_+^2 J_-^2\right)$$
$$+ \frac{\lambda^2}{2}\left(\nabla_-^2 J_+^2 + \nabla_+^2 J_-^2\right)\nabla_\perp^2 - \frac{\lambda^2}{2} J_Z^2 \nabla_\perp^4 - \beta_Z^2\left(J_Z^2 - 1\right)\nabla_\perp^2 + \left(\omega_{TO}^2 - \omega_{LO}^2\right)\left(J_Z^2 - 1\right)$$

Gopalov's Equation

Confined Phonons in 2D Graphene Sheet

$$U(x,y,t) = A\exp\left[i\left(q_n x + q_m y - \omega t\right)\right]$$

$$\omega^2(q) = \begin{cases} \omega_{TO}^2 - \beta_T^2\left(q_x^2 + q_y^2\right) & \ldots \text{TO} \\ \omega_{LO}^2 - \lambda^2\left(q_x^2 + q_y^2\right) + \beta_L^2\left(q_x^2 + q_y^2\right) & \ldots \text{LO} \\ \omega_{ZO}^2 - \beta_Z^2\left(q_x^2 + q_y^2\right) & \ldots \text{ZO} \end{cases}$$

Jun Qian et al.

$$\omega^2(k) = \begin{cases} \omega_{TO}^2 - \beta_T^2 \mathrm{k}^2 & \ldots \mathrm{TO} \\ \omega_{LO}^2 - \lambda^2 \mathrm{k}^4 + \beta_L^2 \mathrm{k}^2 & \ldots \mathrm{LO} \\ \omega_{ZO}^2 - \beta_Z^2 \mathrm{k}^2 & \ldots \mathrm{ZO} \end{cases}$$

Gopalov's results

$$\omega_{TO} = \omega_{LO} = 1581 cm^{-1}, \omega_{ZO} = 893 cm^{-1}$$

$$\beta_L = 7.8 \times 10^5 cm/s, \beta_T = 9.6 \times 10^5 cm/s$$

$$\beta_Z = 7.9 \times 10^5 cm/s, \lambda = 9.3 \times 10^{-3} cm^2/s$$

$$u = 0 \;\; at \;\; x = 0, L$$

$$q_x = q_n = \frac{n\pi}{L}, \;\; q_y = q$$

$$q_{AC} = q_n = \frac{n\pi}{L_{AC}}, \qquad q_{ZZ} = q_m = \frac{m\pi}{L_{ZZ}}$$

Jun Qian et al.

Graphite C-axis Thermal Conductivity

Thin Graphite Sheet: phonon confinement

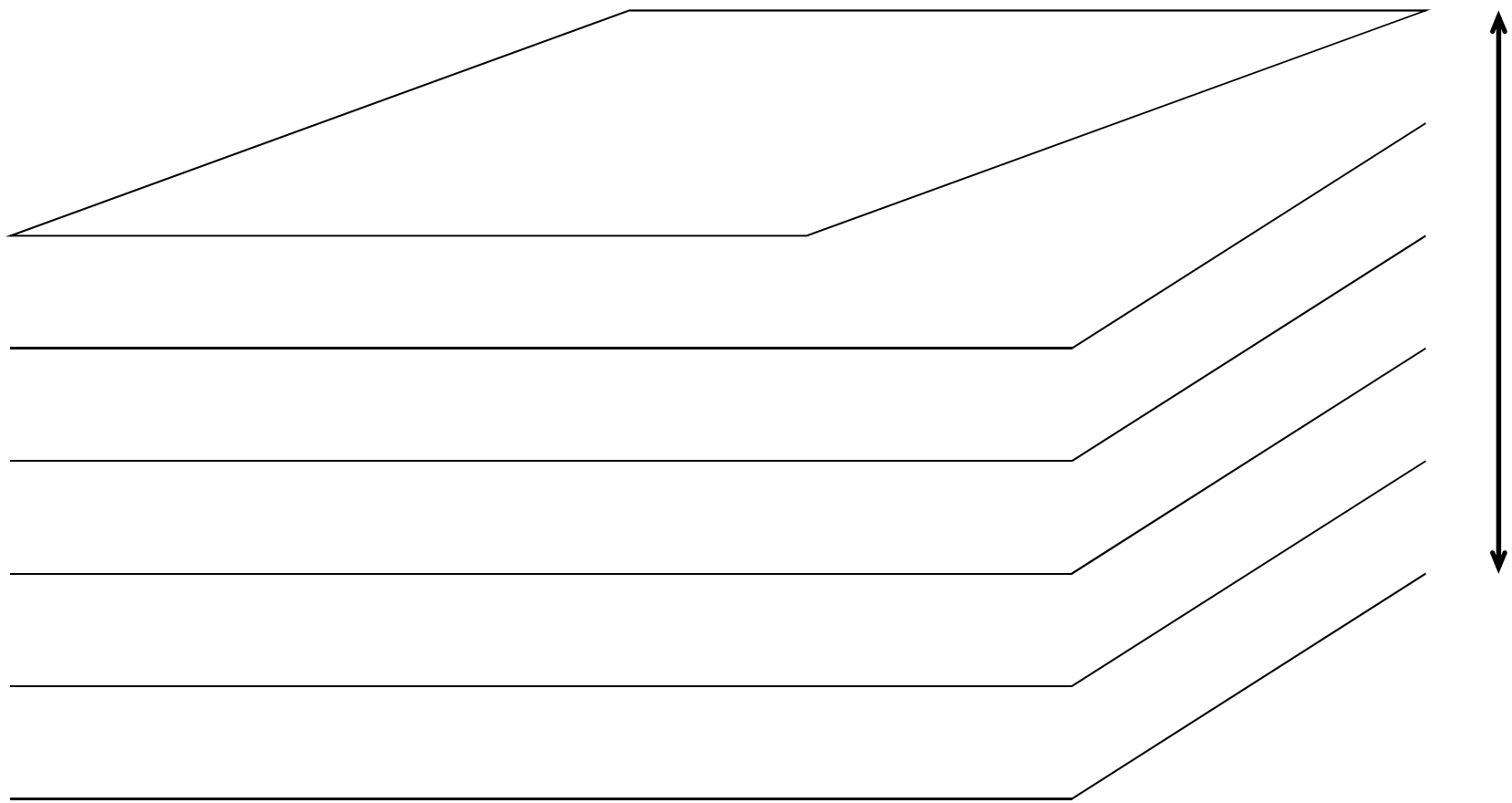

Graphene exhibit high in-plane thermal conductivity, which opens possibility for thermal management in nanoelectronic circuits. Here, instead, we studied the c-axis thermal conductivity. The Klemens model supplemented with phonon mode quantization is used to estimate the thermal conductivity along the c-axis in defect-free graphite that is treated as infinite in the lateral directions but finite (a few planes of graphene) in the c-direction. **As discussed by Klemens, in one dimension the phonon spectral specific heat is**

$$C_1(f) = \frac{kN}{2p\,f_d} = \frac{k}{2p\,f_d} G_1^{\,2} G_3$$

Ke Sun et al.based on formulation of Klemens

$G_3 = 1/a_3$

is the number of layers in a crystal of unit thickness and unit width, each layer having

$G_1^{\,2} = 1/a_2^{\,2}$

is the number of atoms per unit area; accordingly, the number of phonon states is $N = G_1^{\,2} G_3$

The, one-dimensional intrinsic thermal conductivity is given by the usual procedure of integrating this spectral specific heat over the velocity and scattering mean free path; that is,

$$l_i = \int_{f_{lower}}^{f_{upper}} C_1 v l_i df$$

where the lower frequency, f_{lower} and the upper frequency, f_{upper} are determined by the c-axis phonon dispersion relation. For film thicknesses of about 10 nm or less , phonon quantization effects are pronounced and the dispersion relation is discrete in confined directions. f_{upper} = 2.75 THz is the measured value of the upper frequency along the c-axis. Moreover, the lowest possible frequency is given approximately by $f_{lower} = f_{upper}/L$, where L is the number of atoms in the one dimensional chain of carbon atoms, assuming a linear dispersion which is evidently a good approximation from the measured dispersion curve.

Thus, the one dimensional thermal conductivity is given by

$$\lambda_{1D}(T,L) = \frac{\rho}{8\pi\gamma^2}\frac{v^4}{T}\left(\frac{1}{f_{upper}/L} - \frac{1}{f_{upper}}\right) = 1.96331\frac{L-1}{T}\ \mathrm{W/m\cdot K}$$

where $\rho = 2.26\times10^3\ \mathrm{kg/m^3}$ is the density of graphite

$$f_{upper} = 2.75\times10^{12}\ \mathrm{Hz}$$

Ke Sun et al.based on formulation of Klemens

$\gamma^2 = 4$ is the Gruneisen parameter squared, and

v is the out-of-plane group velocity. $v = 932\ \mathrm{m/s}$

v has been taken to be the average of the LA and TA branches , and the upper frequency, f_{upper}, was taken in accord with the measured dispersion relation along the c-axis. The figure depicts the 1D thermal conductivity of a graphite sheet made of 2, 4, 6, and 8 planes of carbon atoms, respectively, as a function of temperature.

Ke Sun et al.based on formulation of Klemens

$$\lambda_{1D}(T,L) = \int_{f_{lower}}^{f_{upper}} \frac{k_B}{2\pi f_d} G_1^2 G_3 v l_i df$$

$$= \frac{\rho v^4}{8\pi^2 \gamma^2 T} \left(\frac{1}{f_{upper}/L} - \frac{1}{f_{lower}} \right)$$

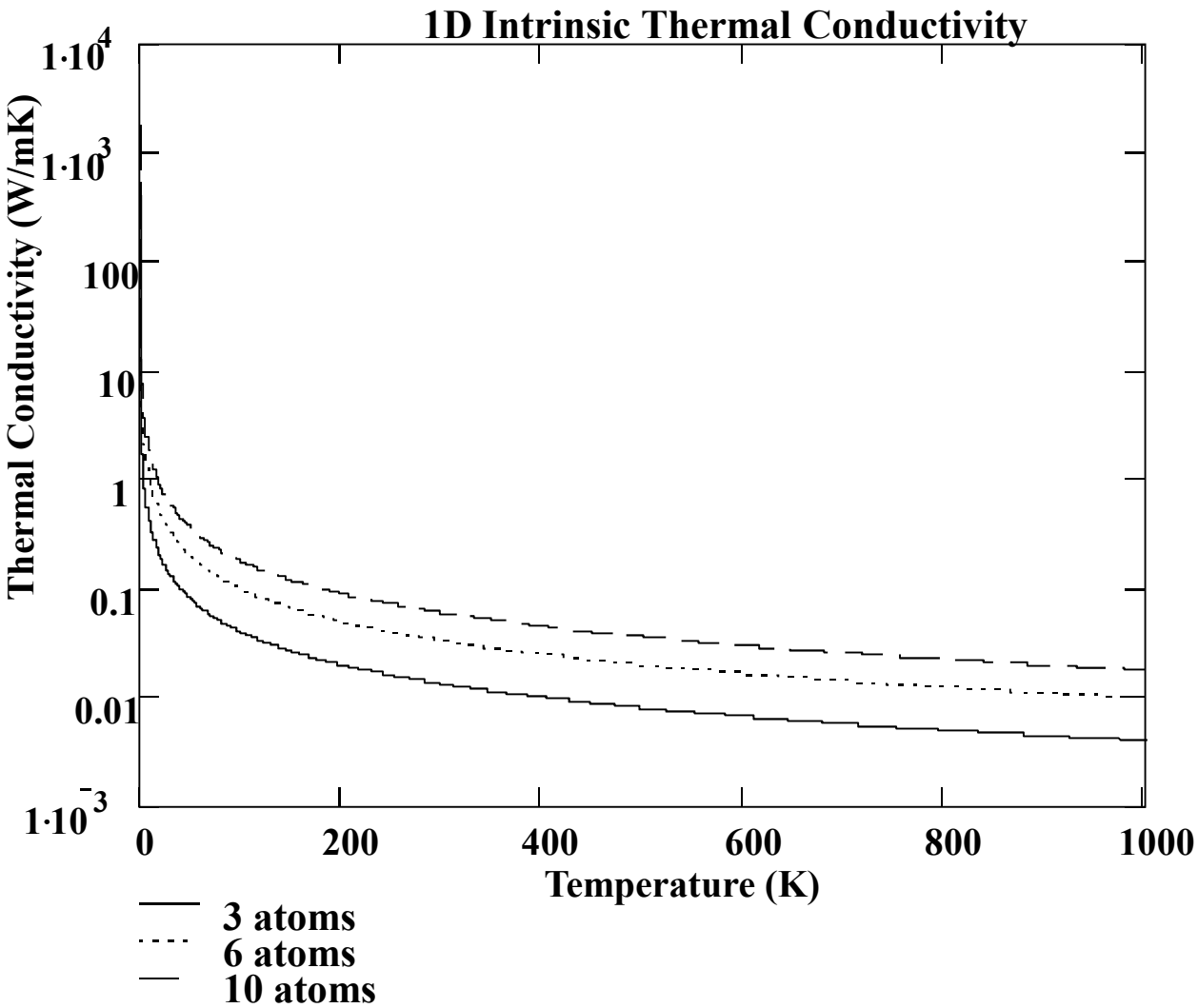

Ke Sun et al.

Figure 65. One dimensional thermal conductivity of c-axis graphite. The solid line is for a chain of 3 graphene planes, the dotted line is for 6 graphene planes, and the dashed line is for 10 graphene planes.

Ke Sun et al.

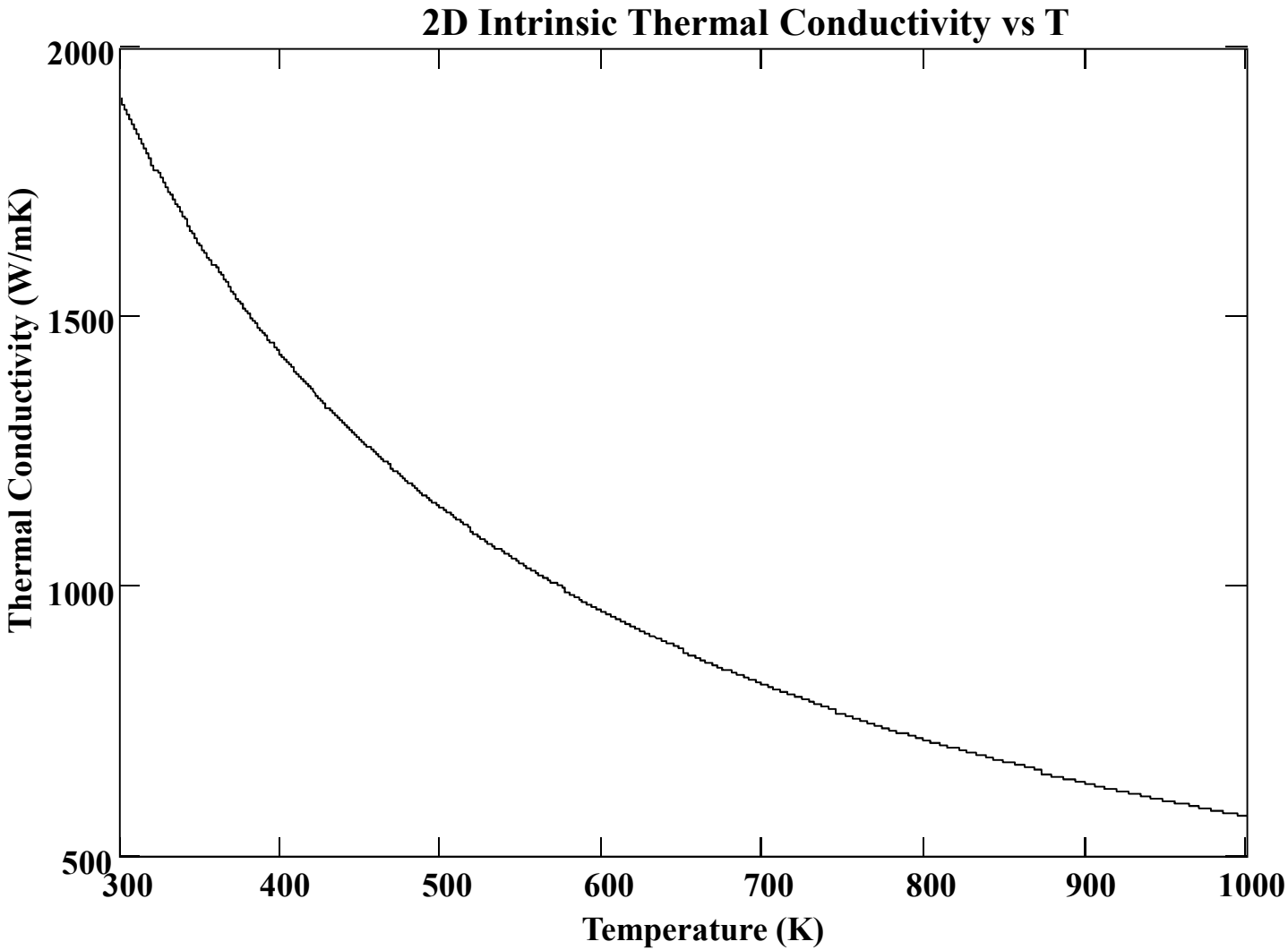
2D Intrinsic Thermal Conductivity vs T
Thermal Conductivity (W/mK)
2000
1500
1000
500
300
400
500
600
700
800
900
1000
Temperature (K)

Ke Sun et al.

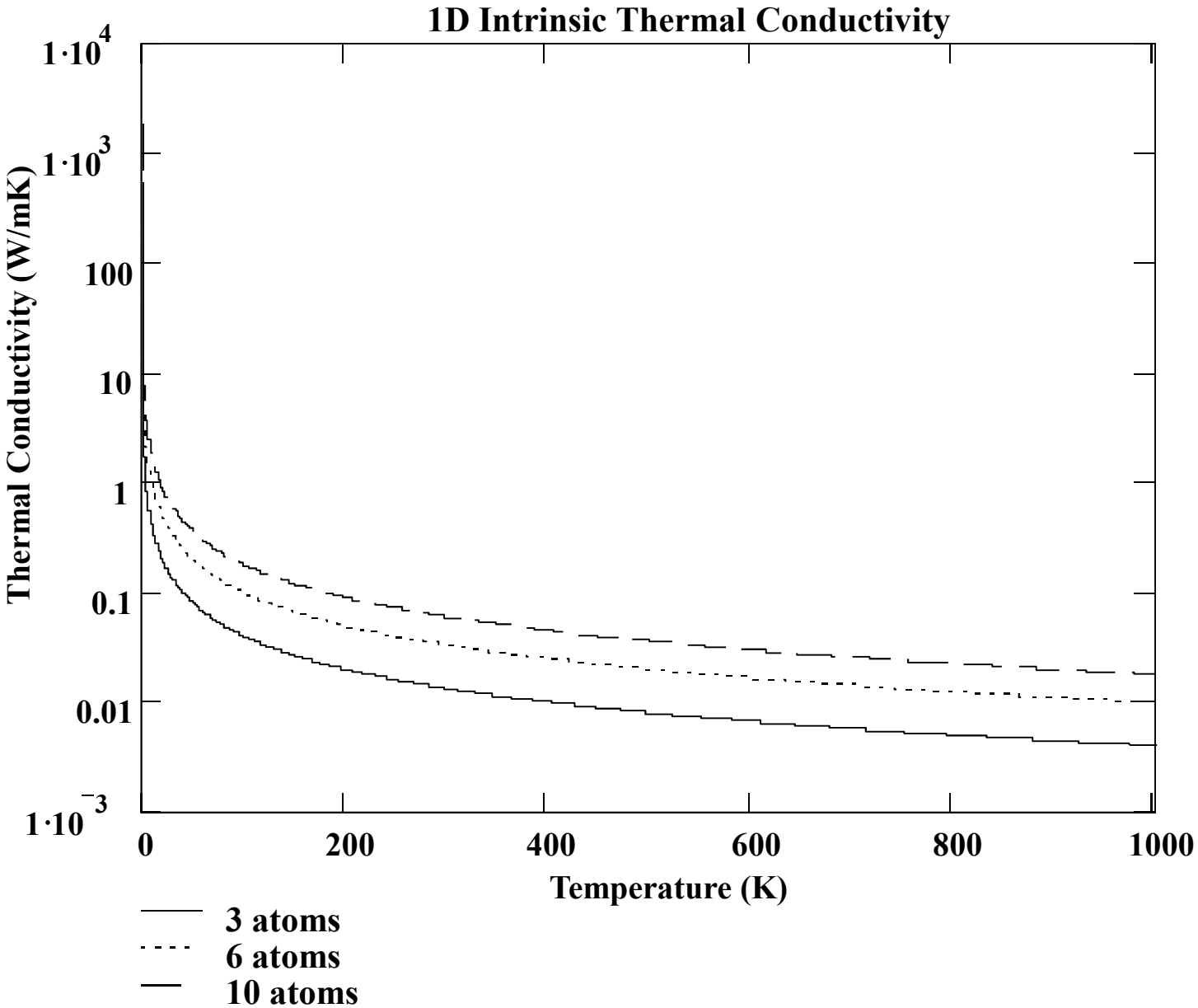
1D Intrinsic Thermal Conductivity
Thermal Conductivity (W/mK)
1·10^4
1·10^3
100
10
1
0.1
0.01
1·10^-3
0
200
400
600
800
1000
Temperature (K)
3 atoms
6 atoms
10 atoms

Ke Sun et al.

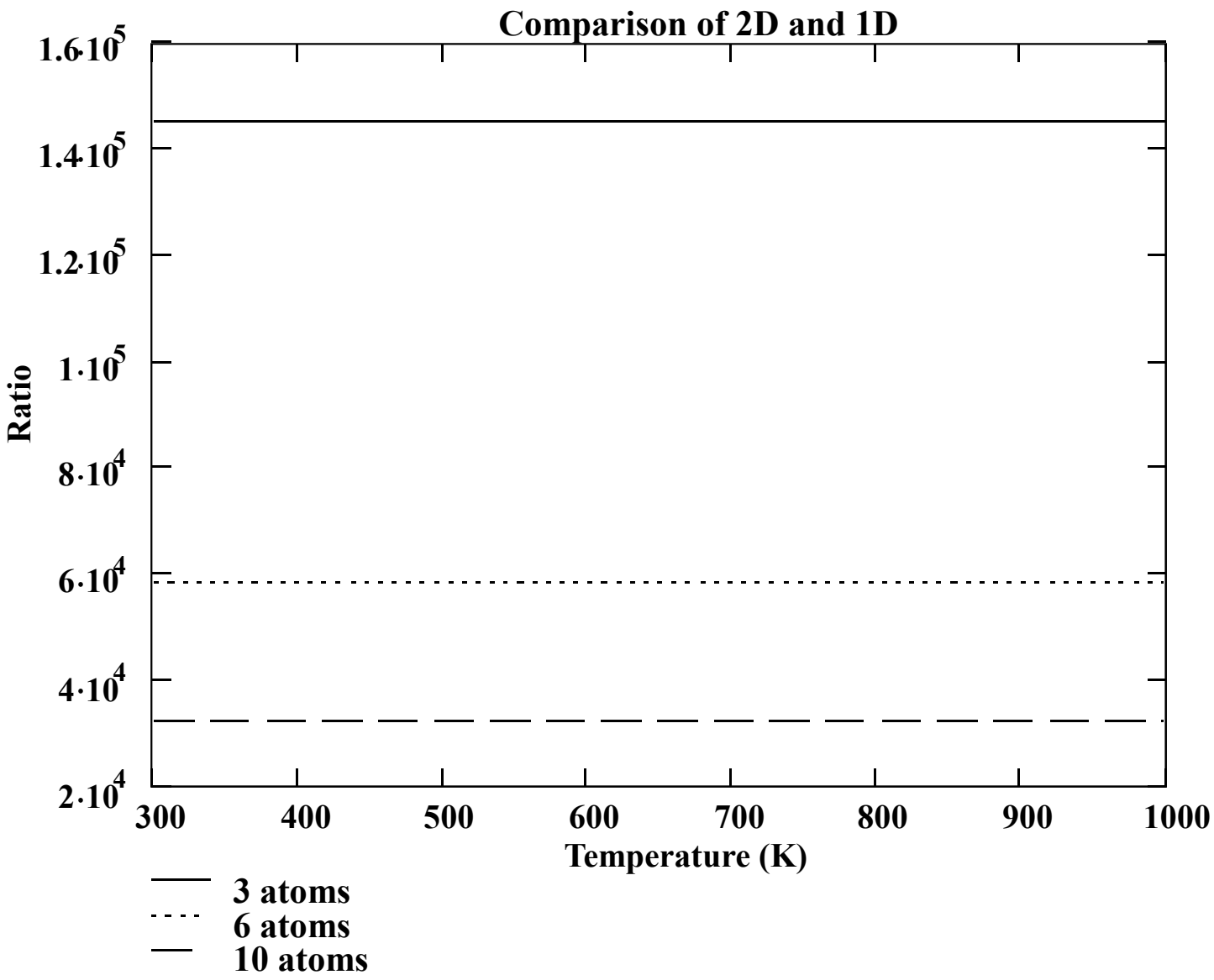
Comparison of 2D and 1D
Ratio
1.6·10^5
1.4·10^5
1.2·10^5
1·10^5
8·10^4
6·10^4
4·10^4
2·10^4
300
400
500
600
700
800
900
1000
Temperature (K)
3 atoms
6 atoms
10 atoms

Enhanced carrier mobilities as a result of reduced carrier-phonon scattering rates in nitride-based systems may be exploited in nitride-based devices as follows:

- use InN-based structures in view of the reduced carrier-phonon interactions (and thus enhanced mobilities) in these systems; a factor of four reduction is expected as compared to AlN based simply on the relative sizes of the Fröhlich coupling constants;

- line broadening associated with the decay of phonons in nitride-based systems of würtzite structure containing point defects; point defects may enhance Raman linewidths, and therefore result in desired reductions, of approximately a factor of two, in a LO phonon lifetimes for nitride-based systems of würtzite structure;

- use metal-semiconductor interfaces or heterostructures having relatively high doping on one side of the heterostructure, may lead to substantial reduction in carrier scattering from the dominant interface modes; this effect is predicted since the electric field of the LO phonon is screened in the metal-like region leading to a boundary condition of vanishing LO phonon field at the interface which effectively eliminated the interface modes since they take on their maximum value at the interface;

- reduce carrier-phonon interactions through the design of $In_xGa_{-x}N$-based structures exhibiting one mode behavior, rather than the nominal two-mode behavior; this approach is based on theoretical predictions --- based on a modified random-element isodisplacement model --- that the A1 and E1 branches in $In_xGa_{-x}N$ exhibit one-mode behavior, as well as experimental results indication one-mode behavior in ternary nitride-based systems. This approach will be combined with effort to exploit the reduced Fröhlich coupling constant in InN-based systems.

- use heterolayers parallel to the current channel that have phonon frequencies that are mismatched with those of the current-carrying-nitride-based materials. The introduction of such layers imposed boundary conditions on the phonons by introduction nodes in mode amplitudes at such layers, thereby resulting in means of engineering the phonon modes and thus the carrier-phonon interactions.

Piezoelectricity in nanowires

PIEZOELECTRIC TENSORS HAVE DIFFERENT FORMS

Wurtzite

$$\overline{e} = \begin{pmatrix} 0 & 0 & 0 & 0 & e_{x5} & 0 \\ 0 & 0 & 0 & e_{x5} & 0 & 0 \\ e_{z1} & e_{z1} & e_{z3} & 0 & 0 & 0 \end{pmatrix} \ldots(1)$$

Zincblende

$$\overline{e} = \begin{pmatrix} 0 & 0 & 0 & e_{x4} & 0 & 0 \\ 0 & 0 & 0 & 0 & e_{x4} & 0 \\ 0 & 0 & 0 & 0 & 0 & e_{x4} \end{pmatrix} \ldots(1b)$$

$$\overline{P} = \overline{e''} \cdot \overline{S}$$

$$V = -\frac{1}{\epsilon - \epsilon_0} \int \overline{P} \cdot d\overline{\rho}$$

$\overline{e}$ ( ) piezoelectric tensor (in cylindrical coordinates), $\overline{P}$ piezoelectric polarization, V piezoelectrically induced potential generated in a nanowire

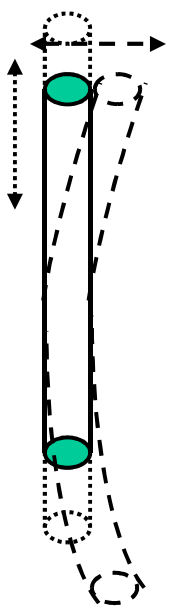

	Zincblende	Wurtzite
Stretching (0.1% strain along z-axis)	Vzz = 0 V (CASE A)	Vzz = - 15.1 V (AlN), - 11.3 V (ZnO) and - 4.9 V (GaN). (CASE C)
Bending (0.1% strain developed along z-axis)	Vrz = 1.4 V (AlN), Vrz = 2 V(ZnO) Vrz = 1 V (GaN) (CASE B)	Vrz = 0.41 V (AlN), 0.41 V (ZnO) and 0.21 V (GaN). (CASE D)

The current literature addresses a large variety of piezo-devices based on over-simplified stress-strain relationships. When the exact piezoelectric tensor is used, the results are dramatically altered in many cases resulting in the magnitude of the piezoelectric effects larger (or smaller) than the published results for bending and stretching of nanowires! It is essential to use the exact piezo tensor as discussed by Sen et al. These effects are discussed in:

Banani Sen, Michael Stroscio, and Mitra Dutta, Piezoelectricity in Wurtzite Polar Semiconductor Nanowires: A Theoretical Study, Journal of Applied Physics, 110, 024506 (2011).

Banani Sen, Michael Stroscio, and Mitra Dutta, Piezoelectricity in Zinc Blende Polar Semiconductor Nanowires: A Theoretical Study, Journal of Applied Physics, 111, in press (2012).

Rocksalt case to come (Banani Sen) …

Selected results are given in the following slides.

Length 1 (along wire at center radius) ~ Fraction of radian times R + a/2

Length 2 (along wire at bottom radius) ~ Fraction of radian times R

Change in Length Along C-Axis (Length 1 – Length 2) ~ Fraction of radian times a/2

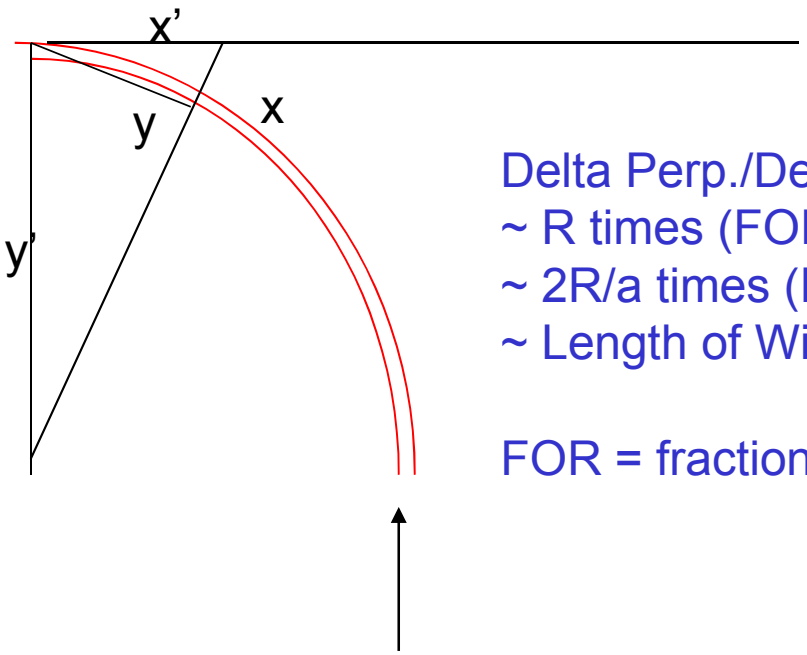

Delta Perp./Delta Parallel
~ R times $(FOR)^2$/ a/2 times FOR
~ 2R/a times (FOR)
~ Length of Wire/Thickness of Wire

FOR = fraction of radian

Thickness, a

x/y ~ x'/y' ~ (Fraction of radian times R)/R = Fraction of radian
y/y' ~ (Fraction of radian times R)/R = Fraction of radian
x/y' ~ $(\text{Fraction of radian})^2$ → x ~ R times $(\text{Fraction of radian})^2$

Wurtzite

Piezoelectric polarization $\overline{P} = \overline{e} \cdot \overline{S}$ and the potential generated $V = -\frac{1}{\varepsilon - \varepsilon_0}\int \overline{P} \cdot d\overline{\rho}$

For materials with wurtzite crystal structure, the piezoelectric tensor in cartesian co-ordinates

$$\bar{e} = \begin{pmatrix} 0 & 0 & 0 & 0 & e_{x5} & 0 \\ 0 & 0 & 0 & e_{x5} & 0 & 0 \\ e_{z1} & e_{z1} & e_{z3} & 0 & 0 & 0 \end{pmatrix}$$

For phonon propagation at an arbitary angle η in XZ plane, the stress tensor transforms to $[e'] = [a][e][\widetilde{M}]$ where $[a]$ is the rotation transformation matrix and $[M]$ is the bond stress transformation matrix derived from .

$$\bar{e}' = \begin{pmatrix} e'_{x1} & e'_{x2} & e'_{x3} & 0 & e'_{x5} & 0 \\ 0 & 0 & 0 & e'_{y4} & 0 & e'_{y6} \\ e'_{z1} & e'_{z2} & e'_{z3} & 0 & e'_{z5} & 0 \end{pmatrix}$$ with

$$e'_{x1} = -e_{z1}\sin\eta\cos^2\eta - e_{z3}\sin^3\eta - e_{x5}\cos\eta\sin 2\eta$$

$$e'_{x2} = -e_{z1}\sin\eta$$

$$e'_{x3} = -e_{z1}\sin^3\eta - e_{z3}\cos^2\eta\sin\eta + e_{x5}\cos\eta\sin 2\eta$$

$$e'_{x5} = -e_{z1}\frac{\sin\eta\sin 2\eta}{2} + e_{z3}\frac{\sin\eta\sin 2\eta}{2} + e_{x5}\cos\eta\cos 2\eta$$

$$e'_{y4} = e_{x5}\cos\eta$$

$$e'_{y6} = -e_{x5}\sin\eta$$

$$e'_{z1} = e_{z1}\cos^3\eta + e_{z3}\cos\eta\sin^2\eta - e_{x5}\sin\eta\sin 2\eta$$

$$e'_{z2} = e_{z1}\cos\eta$$

$$e'_{z3} = e_{z1}\cos\eta\sin^2\eta + e_{z3}\cos^3\eta + e_{x5}\sin\eta\sin 2\eta$$

$$e'_{z5} = e_{z1}\frac{\cos\eta\sin 2\eta}{2} - e_{z3}\frac{\cos\eta\sin 2\eta}{2} + e_{x5}\sin\eta\cos 2\eta$$

In cylindrical polar co-ordinates, $[e''] = [a'][e'][\tilde{M}']$

$$e'' = \begin{pmatrix} e''_{x1} & e''_{x2} & e''_{x3} & e''_{x4} & e''_{x5} & e''_{x6} \\ e''_{y1} & e''_{y2} & e''_{y3} & e''_{y4} & e''_{y5} & e''_{y6} \\ e''_{z1} & e''_{z2} & e''_{z3} & e''_{z4} & e''_{z5} & e''_{z6} \end{pmatrix}$$

with

$$e''_{x1} = e'_{x1}\cos^3\phi + e'_{x2}\cos\phi\sin^2\phi + e'_{y6}\sin\phi\sin 2\phi$$

$$e''_{x2} = e'_{x1}\cos\phi\sin^2\phi + e'_{x2}\cos^3\phi - e'_{y6}\sin\phi\sin 2\phi$$

$$e''_{x3} = e'_{x3}\cos\phi$$

$$e''_{x4} = e'_{y4}\sin\phi\cos\phi - e'_{x5}\sin\phi\cos\phi$$

$$e''_{x5} = e'_{y4}\sin^2\phi + e'_{x5}\cos^2\phi$$

$$e''_{x6} = -e'_{x1}\cos\phi\frac{\sin 2\phi}{2} + e'_{x2}\cos\phi\frac{\sin 2\phi}{2} + e'_{y6}\sin\phi\cos 2\phi$$

$$e''_{y1} = -e'_{x1}\sin\phi\cos^2\phi - e'_{x2}\sin^3\phi + e'_{y6}\cos\phi\sin 2\phi$$

$$e''_{y2} = e'_{x1}\sin^3\phi - e'_{x2}\sin\phi\cos^2\phi - e'_{y6}\cos\phi\sin 2\phi$$

$$e''_{y3} = -e'_{x3}\sin\phi$$

$$e''_{y4} = e'_{y4}\cos^2\phi + e'_{x5}\sin^2\phi$$

$$e''_{y5} = e'_{y4}\sin\phi\cos\phi - e'_{x5}\sin\phi\cos\phi$$

$$e''_{y6} = e'_{x1}\sin\phi\frac{\sin 2\phi}{2} - e'_{x2}\sin\phi\frac{\sin 2\phi}{2} + e'_{y6}\cos\phi\cos 2\phi$$

$$e''_{z1} = e'_{z1}\cos^2\phi + e'_{z2}\sin^2\phi$$

$$e''_{z2} = e'_{z1}\sin^2\phi + e'_{z2}\cos^2\phi$$

$$e''_{z3} = e'_{z3}$$

$$e''_{z4} = -e'_{z5}\sin\phi$$

$$e''_{z5} = e'_{z5}\cos\phi$$

$$e''_{z6} = -e'_{z1}\frac{\sin 2\phi}{2} + e'_{z2}\frac{\sin 2\phi}{2}$$

The strain vector S in cylindrical polar coordinates

$$S_{rr} = \frac{1}{i\omega}\frac{\partial v_r}{\partial r} = \frac{\partial u_r}{\partial r}$$

$$S_{\phi\phi} = \frac{1}{i\omega}\left(\frac{v_r}{r} + \frac{1}{r}\frac{\partial v_\phi}{\partial \phi}\right) = \frac{u_r}{r} + \frac{1}{r}\frac{\partial u_\phi}{\partial \phi}$$

$$S_{zz} = \frac{1}{i\omega}\frac{\partial v_z}{\partial z} = \frac{\partial u_z}{\partial z}$$

$$2S_{z\phi} = \frac{1}{i\omega}\left(\frac{\partial v_\phi}{\partial z} + \frac{1}{r}\frac{\partial v_z}{\partial \phi}\right) = \frac{\partial u_\phi}{\partial z} + \frac{1}{r}\frac{\partial u_z}{\partial \phi}$$

$$2S_{rz} = \frac{1}{i\omega}\left(\frac{\partial v_r}{\partial z} + \frac{\partial v_z}{\partial r}\right) = \frac{\partial u_r}{\partial z} + \frac{\partial u_z}{\partial r}$$

$$2S_{r\phi} = \frac{1}{i\omega}\left(\frac{1}{r}\frac{\partial v_r}{\partial \phi} + \frac{\partial v_\phi}{\partial r} - \frac{v_\phi}{r}\right) = \frac{1}{r}\frac{\partial u_r}{\partial \phi} + \frac{\partial u_\phi}{\partial r} - \frac{u_\phi}{r}$$

Piezoelectrically induced polarization in cylindrical polar coordinates is given as

$$P_r = \left(e'_{x1}\cos^3\phi + e'_{x2}\cos\phi\sin^2\phi + e'_{y6}\sin\phi\sin2\phi\right)\frac{\partial u_r}{\partial r} + \left(e'_{x1}\cos\phi\sin^2\phi + e'_{x2}\cos^3\phi - e'_{y6}\sin\phi\sin2\phi\right)\left(\frac{u_r}{r} + \frac{1}{r}\frac{\partial u_\phi}{\partial\phi}\right)$$

$$+ e'_{x3}\cos\phi\frac{\partial u_z}{\partial z} + \left(e'_{y4}\sin\phi\cos\phi - e'_{x5}\sin\phi\cos\phi\right)\left(\frac{\partial u_\phi}{\partial z} + \frac{1}{r}\frac{\partial u_z}{\partial\phi}\right) + \left(e'_{y4}\sin^2\phi + e'_{x5}\cos^2\phi\right)\left(\frac{\partial u_r}{\partial z} + \frac{\partial u_z}{\partial r}\right)$$

$$+ \left(-e'_{x1}\cos\phi\frac{\sin2\phi}{2} + e'_{x2}\cos\phi\frac{\sin2\phi}{2} + e'_{y6}\sin\phi\cos2\phi\right)\left(\frac{1}{r}\frac{\partial u_r}{\partial\phi} + \frac{\partial u_\phi}{\partial r} - \frac{u_\phi}{r}\right)$$

$$P_\phi = \left(-e'_{x1}\sin\phi\cos^2\phi - e'_{x2}\sin^3\phi + e'_{y6}\cos\phi\sin2\phi\right)\frac{\partial u_r}{\partial r} - \left(e'_{x1}\sin^3\phi - e'_{x2}\sin\phi\cos^2\phi - e'_{y6}\cos\phi\sin2\phi\right)\left(\frac{u_r}{r} + \frac{1}{r}\frac{\partial u_\phi}{\partial\phi}\right)$$

$$- e'_{x3}\sin\phi\frac{\partial u_z}{\partial z} + \left(e'_{y4}\cos^2\phi + e'_{x5}\sin^2\phi\right)\left(\frac{\partial u_\phi}{\partial z} + \frac{1}{r}\frac{\partial u_z}{\partial\phi}\right) + \left(e'_{y4}\sin\phi\cos\phi - e'_{x5}\sin\phi\cos\phi\right)\left(\frac{\partial u_r}{\partial z} + \frac{\partial u_z}{\partial r}\right)$$

$$+ \left(e'_{x1}\sin\phi\frac{\sin2\phi}{2} - e'_{x2}\sin\phi\frac{\sin2\phi}{2} + e'_{y6}\cos\phi\cos2\phi\right)\left(\frac{1}{r}\frac{\partial u_r}{\partial\phi} + \frac{\partial u_\phi}{\partial r} - \frac{u_\phi}{r}\right)$$

$$P_z = \left(e'_{z1}\cos^2\phi + e'_{z2}\sin^2\phi\right)\frac{\partial u_r}{\partial r} + \left(e'_{z1}\sin^2\phi + e'_{z2}\cos^2\phi\right)\left(\frac{u_r}{r} + \frac{1}{r}\frac{\partial u_\phi}{\partial\phi}\right) + e'_{z3}\frac{\partial u_z}{\partial z} - e'_{z5}\sin\phi\left(\frac{\partial u_\phi}{\partial z} + \frac{1}{r}\frac{\partial u_z}{\partial\phi}\right)$$

$$+ e'_{z5}\cos\phi\left(\frac{\partial u_r}{\partial z} + \frac{\partial u_z}{\partial r}\right) + \left(-e'_{z1}\frac{\sin2\phi}{2} + e'_{z2}\frac{\sin2\phi}{2}\right)\left(\frac{1}{r}\frac{\partial u_r}{\partial\phi} + \frac{\partial u_\phi}{\partial r} - \frac{u_\phi}{r}\right)$$

Static permittivity for wurtzite crystals $\varepsilon = \begin{pmatrix} \varepsilon_{xx} & 0 & 0 \\ 0 & \varepsilon_{xx} & 0 \\ 0 & 0 & \varepsilon_{zz} \end{pmatrix}$

On coordinate transformation for phonon propagation at an arbitary angle η

$$\varepsilon'' = [a'][a][\varepsilon][\tilde{a}][\tilde{a}']$$

For no free charge nanowires, piezoelectric potential generated is given by $V = -\frac{1}{\varepsilon'' - \varepsilon_0}\int \overline{P} \bullet d\overline{\rho}$

<u>Piezoelectric stiffening</u>

Elastic stiffness tensor

$$C_{KL}^{E} = \begin{pmatrix} C_{11}^{E} & C_{12}^{E} & C_{13}^{E} & 0 & 0 & 0 \\ C_{12}^{E} & C_{11}^{E} & C_{13}^{E} & 0 & 0 & 0 \\ C_{13}^{E} & C_{13}^{E} & C_{33}^{E} & 0 & 0 & 0 \\ 0 & 0 & 0 & C_{44}^{E} & 0 & 0 \\ 0 & 0 & 0 & 0 & C_{44}^{E} & 0 \\ 0 & 0 & 0 & 0 & 0 & \frac{1}{2}\left(C_{11}^{E} - C_{12}^{E}\right) \end{pmatrix}$$

For phonon propagation at an arbitary angle η, the stiffness matrix transforms as

$$\mathrm{C}'^{\mathrm{E}}_{\mathrm{KL}} = [M][C_{KL}^{E}][\tilde{M}]$$

Results

Strain applied along z-axis, $\frac{\partial u_z}{\partial z}$ is the only non-zero term

$$P_{rzz} = e'_{x3}\cos\phi\frac{\partial u_z}{\partial z} = \left(-e_{z1}\sin^3\eta - e_{z3}\cos^2\eta\sin\eta + e_{x5}\cos\eta\sin 2\eta\right)\cos\phi\frac{\partial u_z}{\partial z}$$

$$P_{\phi zz} = -e'_{x3}\sin\phi\frac{\partial u_z}{\partial z} = -\left(-e_{z1}\sin^3\eta - e_{z3}\cos^2\eta\sin\eta + e_{x5}\cos\eta\sin 2\eta\right)\sin\phi\frac{\partial u_z}{\partial z}$$

$$P_{zzz} = e'_{z3}\frac{\partial u_z}{\partial z} = \left(e_{z1}\cos\eta\sin^2\eta + e_{z3}\cos^3\eta + e_{x5}\sin\eta\sin 2\eta\right)\frac{\partial u_z}{\partial z}$$

$$V_{zz} = -\frac{1}{\varepsilon'' - \varepsilon_0}\left[\int P_{rzz}dr + \int rP_{\phi zz}d\phi + \int P_{zzz}dz\right]$$

On bending wire, $\frac{\partial u_r}{\partial z}$ is the only non-zero term

$$P_{rrz} = \left(e'_{y4}\sin^2\phi + e'_{x5}\cos^2\phi\right)\frac{\partial u_r}{\partial z} = \left(e_{x5}\cos\eta\sin^2\phi + \left(-e_{z1}\frac{\sin\eta\sin 2\eta}{2} + e_{z3}\frac{\sin\eta\sin 2\eta}{2} + e_{x5}\cos\eta\cos 2\eta\right)\cos^2\phi\right)\frac{\partial u_r}{\partial z}$$

$$P_{\phi rz} = \left(e'_{y4}\sin\phi\cos\phi + e'_{x5}\sin\phi\cos\phi\right)\frac{\partial u_r}{\partial z} = \left(e_{x5}\cos\eta\frac{\sin 2\phi}{2} - \left(-e_{z1}\frac{\sin\eta\sin 2\eta}{2} + e_{z3}\frac{\sin\eta\sin 2\eta}{2} + e_{x5}\cos\eta\cos 2\eta\right)\frac{\sin 2\phi}{2}\right)\frac{\partial u_r}{\partial z}$$

$$P_{zrz} = e'_{z5}\cos\phi\frac{\partial u_r}{\partial z} = \left(e_{z1}\frac{\cos\eta\sin 2\eta}{2} - e_{z3}\frac{\cos\eta\sin 2\eta}{2} + e_{x5}\sin\eta\cos 2\eta\right)\cos\phi\frac{\partial u_r}{\partial z}$$

$$V_{rz} = \frac{1}{\varepsilon'' - \varepsilon_0}\left[\int P_{rrz}dr + \int rP_{\phi rz}d\phi + \int P_{zrz}dz\right]$$

Zincblende

Piezoelectric polarization $\overline{P} = \overline{e} \cdot \overline{S}$ and the potential generated $V = -\frac{1}{\varepsilon - \varepsilon_0} \int \overline{P} \cdot d\overline{\rho}$

For materials with wurtzite crystal structure, the piezoelectric tensor in cartesian co-ordinates

$$\bar{e} = \begin{pmatrix} 0 & 0 & 0 & e_{x4} & 0 & 0 \\ 0 & 0 & 0 & 0 & e_{x4} & 0 \\ 0 & 0 & 0 & 0 & 0 & e_{x4} \end{pmatrix}$$

For phonon propagation at an arbitary angle η in XZ plane, the stress tensor transforms to $[e'] = [a][e][\widetilde{M}]$ where $[a]$ is the rotation transformation matrix and $[M]$ is the bond stress transformation matrix derived from .

In cylindrical polar co-ordinates, $[e''] = [a'][e'][\widetilde{M}']$

$$e'' = \begin{pmatrix} e''_{x1} & e''_{x2} & e''_{x3} & e''_{x4} & e''_{x5} & e''_{x6} \\ e''_{y1} & e''_{y2} & e''_{y3} & e''_{y4} & e''_{y5} & e''_{y6} \\ e''_{z1} & e''_{z2} & e''_{z3} & e''_{z4} & e''_{z5} & e''_{z6} \end{pmatrix}$$

with

$$e''_{x1} = -3e_{x4} \sin 2\eta \sin \phi \cos^2 \phi$$
$$e''_{x2} = -e_{x4} \sin 2\eta \sin \phi \left(1 - \cos^2 \phi\right)$$
$$e''_{x3} = e_{x4} \sin 2\eta \sin \phi$$
$$e''_{x4} = e_{x4} \cos 2\eta \cos 2\phi$$
$$e''_{x5} = e_{x4} \cos 2\eta \sin 2\phi$$
$$e''_{x6} = e_{x4} \sin 2\eta \cos \phi \left(2 - 3\cos^2 \phi\right)$$
$$e''_{y1} = -e_{x4} \sin 2\eta \cos \phi \left(1 - 3\sin^2 \phi\right)$$
$$e''_{y2} = -3e_{x4} \sin 2\eta \cos \phi \sin^2 \phi$$
$$e''_{y3} = e_{x4} \sin 2\eta \cos \phi$$
$$e''_{y4} = e_{x4} \cos 2\eta \sin 2\phi$$
$$e''_{y5} = e_{x4} \cos 2\eta \cos 2\phi$$
$$e''_{y6} = -e_{x4} \sin 2\eta \sin \phi \left(1 - 3\cos^2 \phi\right)$$
$$e''_{z1} = e_{x4} \cos 2\eta \sin 2\phi$$
$$e''_{z2} = -e_{x4} \cos 2\eta \sin 2\phi$$
$$e''_{z3} = 0$$
$$e''_{z4} = e_{x4} \sin 2\eta \cos \phi$$
$$e''_{z5} = e_{x4} \sin 2\eta \sin \phi$$
$$e''_{z6} = e_{x4} \cos 2\eta \cos 2\phi$$

The strain vector S in cylindrical polar coordinates

$$S_{rr} = \frac{1}{i\omega}\frac{\partial v_r}{\partial r} = \frac{\partial u_r}{\partial r}$$

$$S_{\phi\phi} = \frac{1}{i\omega}\left(\frac{v_r}{r} + \frac{1}{r}\frac{\partial v_\phi}{\partial \phi}\right) = \frac{u_r}{r} + \frac{1}{r}\frac{\partial u_\phi}{\partial \phi}$$

$$S_{zz} = \frac{1}{i\omega}\frac{\partial v_z}{\partial z} = \frac{\partial u_z}{\partial z}$$

$$2S_{z\phi} = \frac{1}{i\omega}\left(\frac{\partial v_\phi}{\partial z} + \frac{1}{r}\frac{\partial v_z}{\partial \phi}\right) = \frac{\partial u_\phi}{\partial z} + \frac{1}{r}\frac{\partial u_z}{\partial \phi}$$

$$2S_{rz} = \frac{1}{i\omega}\left(\frac{\partial v_r}{\partial z} + \frac{\partial v_z}{\partial r}\right) = \frac{\partial u_r}{\partial z} + \frac{\partial u_z}{\partial r}$$

$$2S_{r\phi} = \frac{1}{i\omega}\left(\frac{1}{r}\frac{\partial v_r}{\partial \phi} + \frac{\partial v_\phi}{\partial r} - \frac{v_\phi}{r}\right) = \frac{1}{r}\frac{\partial u_r}{\partial \phi} + \frac{\partial u_\phi}{\partial r} - \frac{u_\phi}{r}$$

Piezoelectrically induced polarization in cylindrical polar coordinates is given as

$$P_r = -3e_{x4}\sin 2\eta \sin\phi \cos^2\phi \frac{\partial u_r}{\partial r} - e_{x4}\sin 2\eta \sin\phi \left(1-3\cos^2\phi\right)\left(\frac{u_r}{r}+\frac{1}{r}\frac{\partial u_\phi}{\partial \phi}\right)$$
$$+e_{x4}\sin 2\eta \sin\phi \frac{\partial u_z}{\partial z} + e_{x4}\cos 2\eta \cos 2\phi \left(\frac{\partial u_\phi}{\partial z}+\frac{1}{r}\frac{\partial u_z}{\partial \phi}\right) + e_{x4}\cos 2\eta \sin 2\phi \left(\frac{\partial u_r}{\partial z}+\frac{\partial u_z}{\partial r}\right)$$
$$+e_{x4}\sin 2\eta \cos\phi \left(2-3\cos^2\phi\right)\left(\frac{1}{r}\frac{\partial u_r}{\partial \phi}+\frac{\partial u_\phi}{\partial r}-\frac{u_\phi}{r}\right)$$

$$P_\phi = -e_{x4}\sin 2\eta \cos\phi \left(1-3\sin^2\phi\right)\frac{\partial u_r}{\partial r} - 3e_{x4}\sin 2\eta \cos\phi \sin^2\phi \left(\frac{u_r}{r}+\frac{1}{r}\frac{\partial u_\phi}{\partial \phi}\right)$$
$$+e_{x4}\sin 2\eta \cos\phi \frac{\partial u_z}{\partial z} + e_{x4}\cos 2\eta \sin 2\phi \left(\frac{\partial u_\phi}{\partial z}+\frac{1}{r}\frac{\partial u_z}{\partial \phi}\right) + e_{x4}\cos 2\eta \cos 2\phi \left(\frac{\partial u_r}{\partial z}+\frac{\partial u_z}{\partial r}\right)$$
$$-e_{x4}\sin 2\eta \sin\phi \left(1-3\cos^2\phi\right)\left(\frac{1}{r}\frac{\partial u_r}{\partial \phi}+\frac{\partial u_\phi}{\partial r}-\frac{u_\phi}{r}\right)$$

$$P_z = e_{x4}\cos 2\eta \sin 2\phi \frac{\partial u_r}{\partial r} - e_{x4}\cos 2\eta \sin 2\phi \left(\frac{u_r}{r}+\frac{1}{r}\frac{\partial u_\phi}{\partial \phi}\right) + e_{x4}\sin 2\eta \cos\phi \left(\frac{\partial u_\phi}{\partial z}+\frac{1}{r}\frac{\partial u_z}{\partial \phi}\right)$$
$$+e_{x4}\sin 2\eta \sin\phi \left(\frac{\partial u_r}{\partial z}+\frac{\partial u_z}{\partial r}\right) + e_{x4}\cos 2\eta \cos 2\phi \left(\frac{1}{r}\frac{\partial u_r}{\partial \phi}+\frac{\partial u_\phi}{\partial r}-\frac{u_\phi}{r}\right)$$

Static permittivity for wurtzite crystals $\varepsilon = \begin{pmatrix} \varepsilon_{xx} & 0 & 0 \\ 0 & \varepsilon_{xx} & 0 \\ 0 & 0 & \varepsilon_{xx} \end{pmatrix}$

For no free charge nanowires, piezoelectric potential generated is given by $V = -\frac{1}{\varepsilon'' - \varepsilon_0} \int \overline{P} \bullet d\overline{\rho}$

<u>Piezoelectric stiffening</u>

Elastic stiffness tensor

$$C_{KL}^{E} = \begin{pmatrix} C_{11}^{E} & C_{12}^{E} & C_{13}^{E} & 0 & 0 & 0 \\ C_{12}^{E} & C_{11}^{E} & C_{13}^{E} & 0 & 0 & 0 \\ C_{13}^{E} & C_{13}^{E} & C_{33}^{E} & 0 & 0 & 0 \\ 0 & 0 & 0 & C_{44}^{E} & 0 & 0 \\ 0 & 0 & 0 & 0 & C_{44}^{E} & 0 \\ 0 & 0 & 0 & 0 & 0 & \frac{1}{2}\left(C_{11}^{E} - C_{12}^{E}\right) \end{pmatrix}$$

For phonon propagation at an arbitary angle η, the stiffness matrix transforms as

$$C'^{E}_{KL} = [M][C_{KL}^{E}][\widetilde{M}]$$

Results

Strain applied along z-axis, $\frac{\partial u_z}{\partial z}$ is the only non-zero term

$$P_{rzz} = e_{x4} \sin 2\eta \sin\phi \frac{\partial u_z}{\partial z}$$

$$P_{\phi zz} = e_{x4} \sin 2\eta \cos\phi \frac{\partial u_z}{\partial z}$$

$$P_{zzz} = 0$$

$$V_{zz} = -\frac{1}{\varepsilon'' - \varepsilon_0}\left[\int P_{rzz} dr + \int r P_{\phi zz} d\phi + \int P_{zzz} dz\right]$$

On bending wire, $\frac{\partial u_r}{\partial z}$ is the only non-zero term

$$P_{rrz} = e_{x4} \sin 2\eta \sin\phi \frac{\partial u_r}{\partial z}$$

$$P_{\phi rz} = e_{x4} \sin 2\eta \cos\phi \frac{\partial u_r}{\partial z}$$

$$P_{zrz} = 0$$

$$V_{rz} = \frac{1}{\varepsilon'' - \varepsilon_0}\left[\int P_{rrz} dr + \int r P_{\phi rz} d\phi + \int P_{zrz} dz\right]$$